Modeling and Simulation of an Industrial-Scale Parex Process

Marta S. P. Silva and Alírio E. Rodrigues
LSRE—Laboratory of Separation and Reaction Engineering, Dept. de Engenharia Química, Faculdade de Engenharia, Universidade do Porto, Rua do Dr. Roberto Frias, 4200-465 Porto, Portugal

José P. B. Mota
Dept. de Química, Faculdade de Ciências e Tecnologia, Requimte/CQFB, Universidade Nova de Lisboa, 2829-516 Caparica, Portugal

DOI 10.1002/aic.14732
Published online January 27, 2015 in Wiley Online Library (wileyonlinelibrary.com)

The Parex unit for industrial-scale purification of p-xylene was studied through detailed simulation and the accuracy of the developed model tested against real industrial data. Starting from a comprehensive analysis of the construction and operation of the industrial unit, a simulation model was developed that incorporates the existing three major types of dead volumes: bed lines, which connect the beds to the rotary valve, circulation lines, which connect adjacent adsorbent chambers, and bed-head dead volumes, which are located upstream of each bed due to the existence of internals. By gathering operation data and surveys in the pumparound line and in the extract stream, three case studies were defined and compared with simulation results. The model is capable of predicting the performance of the industrial unit. Further simulations were made and compared with plant data to assess the effect of adsorbent capacity loss on the long-term performance of the unit. © 2015 American Institute of Chemical Engineers *AIChE J*, 61: 1345–1363, 2015
Keywords: simulated moving bed, Parex, p-xylene, dead volumes

Introduction

BTX aromatics (benzene, toluene, and xylenes) are mainly produced from reformate, pyrolysis gasoline, and coke oven light oil.[1] Mixed xylenes (*p*-xylene, *m*-xylene, *o*-xylene, and ethylbenzene) can be separated from these streams or can be obtained through toluene disproportionation/transalkylation.

The downstream separation of *p*-xylene from other xylenes and ethylbenzene is a difficult task because of the boiling point similarities between these components (137.7°C for *p*-xylene, 139.0°C for *m*-xylene, 144.0°C for *o*-xylene, and 136.5°C for ethylbenzene at 1 bar).[2] Crystallization and adsorption are the two possible separation principles explored by licensers for the separation of high purity *p*-xylene. Over the years, *p*-xylene adsorption has been widely explored through application of the simulated moving-bed (SMB) technology, sometimes coupled with crystallization under the form of a hybrid separation process.[3,4]

In 1961, UOP patented the Parex process[5] for exploring the adsorptive separation of *p*-xylene. Since then, UOP has licensed dozens of SMB plants[6] and has been improving the faujasitic adsorbent used in the Parex unit.[7] The SMB principle gives a higher *p*-xylene recovery per pass[3] than the crystallization processes that were already in use before the development of the SMB technology.[8]

To understand the separation principle of the Parex process, it is useful to compare it with batch elution chromatography. For this purpose, let us consider a binary feed mixture of components A and B, which have different affinities for an adsorbent packed in a column. The separation of A and B using elution chromatography is done by injecting a pulse of the mixture, in most cases diluted in a suitable solvent, and then eluting the pulse with pure solvent. Given that component A has a higher affinity for the adsorbent than B, A will migrate along the column at a slower rate than component B. If the chromatographic column is long enough, both A and B can be collected pure at the downstream end of the column but at different times. Once the geometric parameters are selected, the design of a binary separation process by elution chromatography is basically the selection of correct values of the pulse duration and frequency and the working flow rate. If the column is overloaded, complete separation of the mixture into pure components A and B may not be possible because the two peaks will frequently overlap. In the case of difficult separations, the system can be operated with recycle or partial fraction collection can be implemented. The important point to note, however, is that using this technique both components are collected at the same point of the system and, therefore, neither continuous feeding nor continuous product withdrawal are possible.

If the solid phase is moved continuously in the opposite direction with respect to the flowing liquid phase and with a velocity intermediate between the migration velocities of A and B, that is, if the solid velocity is higher than the velocity of the concentration front of A and lower than the velocity of the concentration front of B, then both solutes can be separated continuously. Solute B will be collected with the

Correspondence concerning this article should be addressed to Alírio E. Rodrigues at arodrig@fe.up.pt.

liquid at the downstream end of the column, and A will be collected with the solid at the upstream end of the column.

In elution chromatography, the resolution of the peaks is essential for complete separation of the components: high purity is only achieved when high peak resolution is possible and thus the peaks can be completely separated. Using a moving bed, however, the total separation of the peaks is only required at both ends of the concentration profiles. Moreover, with a moving bed the capacity of the adsorbent is further used, which contributes for higher productivities.

The direct application of the principle explained above is best exploited in an ideal process termed true moving bed (TMB), which consists of a train of four countercurrent chromatographic columns arranged in a closed loop. While the solid flows continuously along the entire system, the liquid flow rate changes between columns due to the presence of two inlet ports—feed and desorbent—and two outlet ports—raffinate and extract.[9] In Parex process, *p*-xylene is the component with higher affinity for the adsorbent and is, thus, recovered in the extract. The other isomers—*m*-xylene and *o*-xylene—and ethylbenzene are recovered in the raffinate.

The physical realization of the TMB concept is hindered by extreme difficulty to implement a steady, uniform movement of a packed solid phase, namely the difficulty to maintain plug-flow of the solid particles, the abrasion of the particles against the column wall and ancillary equipment, and the formation of fines due to friction between particles.

The SMB process was cleverly developed as an effective and efficient means of implementing the TMB principle. In the SMB, the solid is stationary; its movement is simulated by dividing each zone of the TMB into one or more packed columns and shifting the positions of the four ports periodically and synchronously in the direction of the fluid flow. The TMB model, although unpractical, remains a useful tool for understanding and modeling the SMB unit, because it is the limiting case of the SMB model for an infinite number of columns with differential bed length and infinitely small switching time.

As discussed above, the most widely used TMB/SMB configuration uses four zones, each separated by an inlet and an outlet port:

- Zone I is the zone between the feed inlet port and the raffinate outlet port. In this zone, the more adsorbed component is adsorbed (to flow with the solid) and the less adsorbed component is desorbed (to flow with the liquid); the task of this zone is to prevent the more adsorbed component from reaching the raffinate port.
- Zone II is located between the extract outlet port and the feed inlet port. This zone prevents the less adsorbed component from reaching the extract port, thus avoiding the contamination of the extract. Here, the more adsorbed component is desorbed (to flow with the liquid) and the less adsorbed component is adsorbed (to flow with the solid);
- Zone III is located between the desorbent inlet port and the extract outlet port, and its function is to regenerate the adsorbent, that is, to prevent the more strongly adsorbed species from reaching Zone IV;
- Zone IV is located between the raffinate outlet port and the desorbent inlet port, and it has the function of regenerating the desorbent. At the downstream end of this zone, the cleaned desorbent can be recycled to Zone III.

The Parex process[10] operates according to the SMB principle, by means of a rotary valve that synchronously switches the ports in the direction of the fluid flow, but uses a seven-zone configuration because it uses seven streams: three inlets—feed, desorbent, and flush in—and four outlets—extract, raffinate, flush out, and recycle/secondary flush; these streams are described in detail in Description of an Industrial Parex Unit section. Besides the particulars of the seven-zone configuration, a comprehensive model-based description of the Parex process must take into account all the dead volumes that have a size large enough to alter the performance of the unit.

Some authors have already considered the effect of dead volumes on SMB units, although not always with respect to the separation of *p*-xylene by the Parex process.[11–14] In the case of the Parex unit, Minceva and Rodrigues[15] studied the effect of the bed lines; these authors calculated the concentration in the volume of liquid trapped in the transfer line by averaging the plug-flow concentration profile during the last stage of its previous use (using a definition of three moments in the operation of the transfer lines) and used the continuous stirred tank model to model the transfer lines between two consecutive uses. Lim et al.[16] considered the existence of bed lines, circulation lines, and bed-head dead volumes, and all dead volumes were considered to have the same diameter as the adsorptive beds. Recently, Sutanto et al.[17] considered three different types of dead volumes in their model of the Parex unit, and compared an eight-zone unit with the Parex's seven-zone configuration.

In this work, a specific industrial-scale Parex unit is modeled with the goal of predicting its performance. The unit's flow sheet is studied in detail and the developed model accounts for all the relevant dead volumes in the unit. The extract history and the internal concentration profile measured in the real unit are compared with the simulation results. Finally, the effect of adsorbent capacity loss over the years is analyzed for one of the case studies.

Description of an Industrial Parex Unit

To obtain an extract stream enriched in *p*-xylene and a raffinate stream depleted of *p*-xylene, the commercial Parex unit uses 24 adsorbent beds divided into two chambers. Each adsorbent chamber has 12 beds and each bed is connected to the rotary valve as depicted in Figure 1. The liquid circulates between the two adsorbent chambers through the pusharound and pumparound (PA) lines, which connect, respectively, beds 12 (Column 1) and 13 (Column 2), and beds 24 (Column 2) and 1 (Column 1).

In the commercial Parex unit, the adsorbent beds are divided into seven-zones, named I, IIA, II, IIB, III, IIIA, and IV, instead of the standard four-zones. The existence of three extra zones is due to the fact that the same bed lines are used to inject and to withdraw streams, thereby generating dead volumes that would contaminate the streams flowing in those lines during the subsequent switching interval if no countermeasures were taken. To avoid these problems, three ports are added in the rotary valve for flushing streams (Figure 1).

The rotary valve, patented by UOP in 1962,[18] switches periodically and synchronously the seven inlet/outlet ports of the unit in the direction of the fluid flow. The valve rotates by $360°/24 = 15°$ every switching interval, t^*, which is between 1 and 2 min depending on the operating conditions. The zone configuration of the Parex unit is 7-2-6-1-4-1-3 [I, IIA, II, IIB, III, IIIA, and IV] (the equivalent four-zone configuration would be 7-9-5-3).

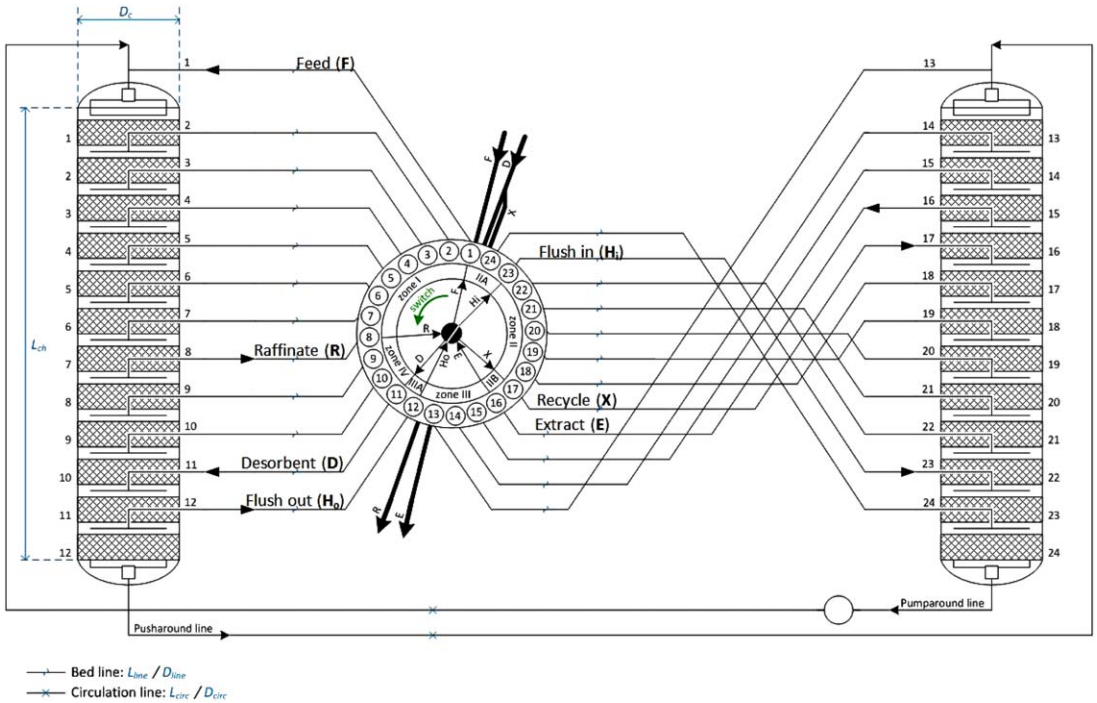

Figure 1. Diagram of the Parex unit, with 12 columns per adsorbent chamber connected to a single rotary valve, organized in a seven-zone configuration.

[Color figure can be viewed in the online issue, which is available at wileyonlinelibrary.com.]

The three streams used for washing the lines are:

Primary flush out

The separation of Zones II/III and III/IV is done by, respectively, withdrawing the extract and injecting the desorbent streams. If the desorbent were injected directly through a line previously used to withdraw the extract, the desorbent stream would be contaminated with *p*-xylene, which would increase its quantity in the raffinate and consequently reduce the recovery of *p*-xylene in the unit. It is important to note that the reduction of *p*-xylene recovery in the Parex unit decreases the conversion in the isomerization reactor (Isomar unit) located downstream in the process. To decrease the contamination of the desorbent by the extract stream, the line that in the next switching interval will be used to inject the desorbent stream is washed by removing the volume (or a fraction of it) that is held back in the line and injecting it in Zone II (zone of separation of *p*-xylene). As previously mentioned, the primary flush out stream is taken from the bed that is immediately upstream of the desorbent injection port; this one-column zone between the primary flush out port and the desorbent port is named Zone IIIA.

Primary flush in

Given that the primary flush stream, which is withdrawn at a position located between the extract and desorbent ports, contains *p*-xylene, it must be injected again into the unit, otherwise, the recovery decreases. The primary flush stream is injected into Zone II, between the feed and extract ports, more precisely, two columns ahead of the feed port. The primary flush also pushes into the column the feed volume that remained in the lines after injection, thereby avoiding the contamination of the extract and the loss of feed. The injection of the primary flush separates Zones II and IIA.

Secondary flush or recycle

A secondary flush is injected between the primary flush injection and the extract port to guarantee that the line used to remove the extract is clean. The secondary flush or recycle is a small desorbent stream diverted from the main desorbent stream after passing through the filters of the desorbent. The secondary flush makes a second wash of the line that will be used to withdraw the extract, by filling it with *p*-diethylbenzene, and therefore, it guarantees that the extract is removed without any contamination. The secondary flush port separates Zones II and IIB, and is connected to the bed upstream of the extract port.

The adsorbent chambers operate at 177°C and approximately 8.8 kg/cm^2. The adsorbent chamber's I.D. is 4.267 m and the total height without the elliptical heads, L_{ch}, is 13.535 m (measured between the top of section 1 or 13 and the bottom of section 12 or 24). A section of the adsorbent chamber consists of an adsorbent bed, the grid and support grid beams, and the internal piping.

The dimensions of the internals were analyzed in detail, and if the height of each section is measured between the bottom of the grids above and below each bed, then the volume available for the adsorbent is equal in all beds, as is the dead volume created by the existence of internals.

To model the different parts of the adsorbent chambers, the dimensions of the dead volumes of the internal piping, grid, and grid support beams were estimated and subtracted from the total section volume for calculating the volume available for the adsorbent.

Figure 2 shows a simplified representation of a section of the adsorbent chamber, which is the building block of our model. This basic block is repeated 24 times to create the Parex unit; a dead volume is inserted between beds 12/13 and beds 24/1 corresponding to the pusharound and pumparound (PA)

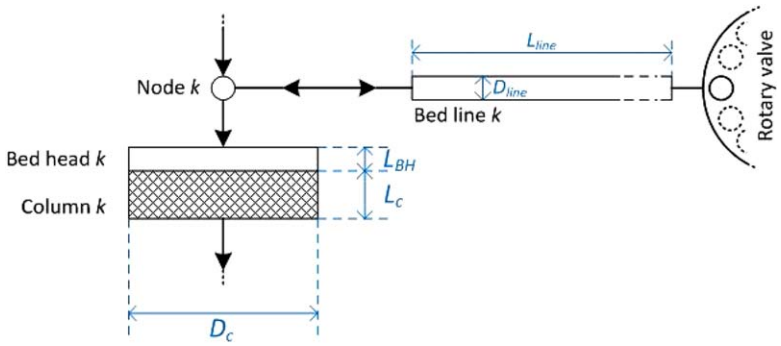

Figure 2. Simplified schematic of an adsorbent chamber: bed, bed head, injection/withdrawal node, and connection to the rotary valve through a bed line.

[Color figure can be viewed in the online issue, which is available at wileyonlinelibrary.com.]

circulation lines. The length of the lines was estimated based on the height of the adsorbent chamber without the heads, 13.535 m, the height of each head (top and bottom), 1.938 m, the distance between the inlet/outlet point and the side of the adsorbent chamber (adsorbent chamber radius), 2.134 m, and approximately 3 m for the distance between the adsorbent chambers. It should be noted that the volumes of the pipe distributors to the top grid and from the bottom grid (approximately 0.15 and 0.29 m^3) were included in the volume of the circulation lines; it was assumed that the distributors have the same diameter as the circulation lines and that their length is equal to the height of each elliptical head. A length of 25 m was considered for the circulation lines.

In the PA line, a PA controller keeps each zone flow rate constant as the zone moves around the adsorption circuit. The PA control is based on zone equations written as a function of the rotary valve position at any given time. The position of the rotary valve is usually defined by reference to the position of the feed stream.

Because for all practical purposes the flowing liquid is incompressible, fixing the flow rate in one zone necessarily fixes the flow rates in all zones because at each inlet or outlet point, the zone flow rate downstream of that point is equal to the upstream flow rate plus or minus whatever flow rate is added or removed at that point.

In the simplified schematic of a section, shown in Figure 2, the volume of the internal piping for intermediate grids ($V_{piping} = 0.03$ m^3) was considered to be part of the bed lines. It should be pointed out that the volume of the internal piping is small when compared to the volume of the section (approximately 0.2%). The dimensions of the bed lines, which are all equal, are given in Table 1 along. Figure 2 also shows the node representing the injection/withdrawal point where the inlet/outlet mass balances are applied. Table 1 summarizes the relevant dimensions of the industrial-scale Parex unit along with some adsorbent characteristics.

The total weight of adsorbent loaded into the Parex unit was 279,682 ton (1880 drums). Using the total volume of the adsorbent chambers available for the adsorbent (312.3 m^3), the bulk density, ρ_{bulk}, of the beds is determined by

$$\rho_b = \frac{m_{ads}}{V_c} \tag{1}$$

Assuming that ρ_{bulk} is equal in all beds then the obtained value is $\rho_b = 896$ kg/m^3. The porosity of the beds is assumed constant and given by

$$\rho_p = \frac{\rho_b}{1-\varepsilon_b} \tag{2}$$

Procedures for Evaluation of the Parex's Performance During Operation

PA surveys and extract-out surveys are commonly used tests to evaluate the performance of the Parex unit during operation. The procedures followed in the plant for obtaining PA and extract surveys are presented below.

PA survey

The PA survey is a series of 24 samples taken from the PA circulation line at different times over one full cycle of the rotary valve. The analysis of these samples gives the composition profile in each zone as it passes through the PA loop. The results of the PA survey are useful data for

Table 1. Characteristics of the Industrial-Scale Parex Unit

Adsorbent Chamber							Dead Volumes		
No. beds/adsorbent chamber						12	Bed head	L_{BH}, m	0.22
D_c (I.D.), m						4.267		D_{BH}, m	4.267
L_{ch}, m						13.535	Bed lines	L_{line}, m	17.76
L_c, m						0.91		D_{line}, m	0.127
							Circulation lines	L_{circ}, m	25.00
								D_{circ}, m	0.203
Rotary valve (configuration)							Unit's selective and nonselective volumes		
I	IIA	II	IIB	III	IIIA	IV	V_s, m^3		48.11
7	2	6	1	4	1	3	V_w, m^3		239.70
Adsorbent									
m_{ads}^{total}, kg				279,682			ρ_b, kg/m^3	896	
ε_b				0.39			ρ_p, kg/m^3	1480	
ε_p				0.36			R_p, mm	0.31	

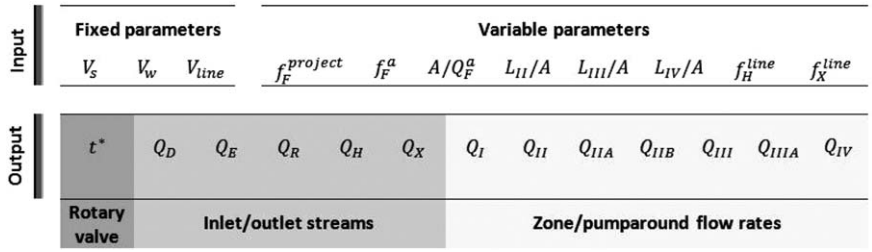

Figure 3. Operating parameters—inputs introduced by operators and outputs for the process.

troubleshooting purity and/or recovery problems and to optimize the unit.

The sampling procedure is important as the composition is constantly changing at the PA; at a fixed sampling location, the composition of the PA stream at the start of the rotary valve step is different from the composition of the PA stream at the end of the step, which is especially true for positions adjacent to process streams. Therefore, each bed should be sampled at the same point in time during a given step for consistency. A good approach is to take each sample approximately at the middle of the step.

One sample was taken for each Feed Inlet Position (FIP) of a complete cycle of the rotary valve cycle, giving a total of 24 samples. The samples were analyzed according to the standard test method ASTM D5917-09.

Extract-out survey

The survey of the extract stream is used to evaluate the *p*-xylene purity obtained over one complete cycle. It is represented as function of the FIP or of the extract outlet position, [EOP] (EOP = FIP − 9 for FIP > 9; EOP = FIP + 15 for FIP < 10), and ideally it should be uniform along the 24 positions of the cycle. For taking samples at the extract outlet, a sampling procedure similar to the one applied in the PA circulation line is followed.

Definition of Operating Parameters

The operation of the SMB plant is dependent on the control of the flow rates (feed, desorbent, extract, raffinate, flush in/out, and recycle or secondary flush), switching time, and the flow rate of water that is injected into the desorbent stream to maintain the hydration level of the adsorbent. These parameters are inputs of the unit and can be changed by the operators.

The calculation of the stream flow rates, Q_j (m^3/h), and switching time, t^* (h), is based on fixed and variable parameters (Figure 3).

The fixed parameters are the selective and nonselective volumes of the unit, V_s (m^3) and V_w (m^3), which are directly connected to the volume of the unit and to the volume of adsorbent, and the volume of the bed lines, V_{line} (m^3).

The other parameters are directly changed by the operator. The feed flow rate is specified in the unit's control system as a percentage of the project value, $f_F^{project}$, which has a fraction of C_8 aromatic hydrocarbons associated, f_F^a. The project flow rate, $Q_F^{project}$, of the industrial unit in study is 107.5 m^3/h. A/Q_F^a is a design parameter related to the simulated velocity of the solid and the velocity of the liquid; it gives the ratio between the selective volume of the solid contained in the unit and the aromatic liquid volume of the feed injected into the unit per cycle. A (m^3/h) is the rate of simulated circulation of the selective adsorbent pore volume and Q_F^a is the volumetric rate of feed stream containing the mixture of C_8 alkylaromatic hydrocarbons.

The fraction of the bed lines washed during flush in/out (H) and recycle or secondary flush (X), respectively, f_H^{line} and f_X^{line}, are also input parameters. The flow rates of Zones II, III and IV (Q_{II}, Q_{III}, and Q_{IV}) are input parameters; in the case of the operation of the industrial unit, they are specified using A as a scaling factor, that is, they are specified in the control console as L_{II}/A, L_{III}/A, and L_{IV}/A, see Eqs. 11–13.

The required calculations to determine the primitive operating parameters are given below. The feed flow rate of aromatics, Q_F^a, is determined from the ratio of the working and projected feed flow rates, $f_F^{project}$, and the fraction of aromatics in the feed stream, f_F^a

$$Q_F = Q_F^{project} f_F^{project} \tag{3}$$

$$Q_F^a = Q_F f_F^a \tag{4}$$

The feed flow rate of aromatics is then used to determine the required flow rate of simulated circulation of the selective adsorbent pore volume, A, to achieve an effective separation

$$A = \varepsilon_\mu \; Q_{solid}^{TMB} = \left(A/Q_F^a\right) Q_F^a \tag{5}$$

which is turn defines the duration of a full cycle, t_c

$$A = \frac{V_s}{t_c} \tag{6}$$

Knowing the cycle time, t_c (h), given by Eq. 6, the port switching time t^* (h), is determined by dividing t_c by the number of columns, which, in this case, is 24

$$t^* = \frac{t_c}{24} \tag{7}$$

The switching time, t^*, is used directly to calculate the flow rates of the flush in/out streams, Q_H (Q_{H_i} or Q_{H_o}), and of the recycle stream (secondary flush), Q_X

$$Q_H = \frac{f_H^{line} V_{line}}{t^*} \tag{8}$$

$$Q_X = \frac{f_X^{line} V_{line}}{t^*} \tag{9}$$

The calculation of the inlet/outlet flow rates and zone flow rates is based on the three input parameters L_{II}/A, L_{III}/A, and L_{IV}/A, through Eqs. 10–20. The flow rate calculation uses the nonselective volume of the unit, V_W, which includes the nonselective voids of the bed, grids, and circulation piping, to define a flow rate W equal to the volume of liquid

required to displace any solute present in the nonselective void volume of the equivalent TMB unit per cycle

$$W = \frac{V_W}{t_c} \tag{10}$$

$$Q_{II} = (L_{II}/A) \times A + W \tag{11}$$

$$Q_{III} = (L_{III}/A) \times A + W \tag{12}$$

$$Q_{IV} = (L_{IV}/A) \times A + W \tag{13}$$

$$Q_{IIA} = Q_{II} + Q_H \tag{14}$$

$$Q_I = Q_{IIA} + Q_F \tag{15}$$

$$Q_{IIB} = Q_{II} - Q_X \tag{16}$$

$$Q_{IIIA} = Q_{III} + Q_H \tag{17}$$

$$Q_D = Q_{IIIA} - Q_{IV} \tag{18}$$

$$Q_E = Q_{III} - Q_{IIB} \tag{19}$$

$$Q_R = Q_I - Q_{IV} \tag{20}$$

The volumetric flow rate of the raffinate stream can be used to check the material balances, because $Q_R = Q_F + Q_D + Q_X - Q_E$

The calculations above neglect the influence of the bed heads on the operation of the unit. As the dead volumes of the elliptical heads of the adsorbent chambers can be a source of contamination, small desorbent streams purged after the desorbent filters are injected into the top and bottom of the adsorbent chambers. These streams are then mixed with the fluid inside the adsorbent chambers and collected in the outlet streams of the unit with the rest of the desorbent. The flow rate of these streams is equal to the minimum flow rate that ensures the absence of contamination. The adsorbent chamber heads should be filled with at least 99% of *p*-diethylbenzene.

The water injection is not included in the calculations above as the correct hydration level of the adsorbent is already taken into account in the adsorption parameters of the model.

Modeling of the Industrial SMB Unit

Many authors have applied the powerful equilibrium theory to the design of the SMB (TMB approach[19–22]/SMB approach[23,24]), which neglects the mass-transfer resistances and axial dispersion, and considers the columns to have an infinite efficiency.[25] Although adsorption rate limitations may introduce significant modifications in the form of the chromatographic concentration profiles, they do not change the qualitative picture of the separation region. As in most industrial SMB processes the chromatographic behavior is governed by the adsorption equilibrium, the equilibrium theory presents a useful qualitative guide of the behavior of the adsorption process.[26]

To get a quantitative description of most SMB processes, however, it is necessary to consider the influence on band broadening of a finite adsorption rate and dispersion effects. Thus, in the majority of the literature references, the TMB or SMB models are based on equilibrium or rate-based versions of the dispersed plug-flow model of an adsorption column to simulate a SMB unit. The equations that define these models result from material balances, and in some instances (e.g., gas-phase applications) also of energy and momentum balances, over a differential volume element of the bed, coupled with a more or less detailed model of the adsorption rate at the particle level. This is the approach followed in this work to model the industrial-scale SMB unit.

The SMB model of the Parex unit requires the definition of the fixed-bed model, the balances at the nodes that connect each pair of consecutive beds for the definition of the inlet/outlet ports, and the description of the unit's dead volumes. The submodels developed for the simulation of the Parex unit are described next.

We have recently characterized the adsorption equilibria and kinetics of the main components of the Parex process—ethylbenzene, *p*-diethylbenzene, *p*-xylene, *m*-xylene, *o*-xylene, and toluene—on a Ba-exchanged faujasite-type zeolite similar to that used in the industrial process.[27–29] The batch[29] and fixed-bed experiments[27] were performed at the operating conditions of the industrial unit (177°C and 9 bar). Prior to each batch experiment, the adsorbent was pretreated under humid helium flow to control its hydration level.[29] The experimental adsorption equilibrium data were successfully fitted to Langmuir-type isotherms. Moreover, it was found that a mass-transfer model in which the macropore diffusion is the rate-controlling mechanism satisfactorily describes the experimental uptake curves.

Fixed-bed submodel

Depending on whether the model is described by a TMB or SMB approach, submodels of a countercurrent adsorbent bed, with countercurrent flow of the solid with respect to the liquid, or a fixed-bed, should be used, respectively. As this section is dedicated to the development of a complete SMB model for the industrial Parex unit, only the fixed-bed submodel is presented. A reduced-order TMB model of the Parex unit is presented below while discussing the simulation results and plant data.

In this work, the mass-transfer resistances are lumped into a single overall resistance, which is kept separate from the contribution of axial dispersion. The former is modeled using a lumped approach based on the linear-driving-force (LDF) approximation proposed by Glueckauf,[30] which has been extensively used in the SMB field (TMB approach[9,31–38]/SMB approach[36,39–46]). The validity of the LDF approximation in sorption processes was studied by Rodrigues and Dias,[47] and some authors have proposed extensions of the LDF approximation to account for mass-transfer resistances in bidisperse adsorbents.[48] As stated above, our LDF coefficients are essentially governed by macropore diffusion as it is the rate-controlling mechanism.[29]

The mass balance for the *i*th component i ($i = 1, \ldots, NC$) in the interparticle fluid is

$$\frac{\partial C_{ij}}{\partial t} + u_j \frac{\partial C_{ij}}{\partial z} + \frac{1-\varepsilon_b}{\varepsilon_b} k_i \left(C_{ij} - \bar{C}_{pij}\right) = D_{ax} \frac{\partial^2 C_{ij}}{\partial z^2} \tag{21}$$

where j is the bed number ($j = 1, ., 24$), C_{ij} (mol/m^3) is the concentration in the bulk of the interparticle fluid, $\bar{C}_{pij}$ (mol/m^3) is the average fluid-phase concentration in the macropore volume of the pellets, u (m/s) is the interstitial fluid velocity, k_i (s^{-1}) is the LDF mass-transfer coefficient, D_{ax} (m^2/s) is the axial dispersion coefficient, and ε_b is the interparticle porosity.

The fluid velocity is considered constant along the column's axial coordinate because the dependence of u on the liquid composition is very mild and a detailed description of the axial velocity profile increases considerably the computational overhead of simulating a multicomponent, multibed

Table 2. Plant Operating Parameters for the Three Case Studies and Information About the Type of Surveys Available for Comparison Against the Simulation Results

Case	A	B	C
$f_F^{project}$	0.9247	1.1500	0.9500
f_F^a	0.935	0.935	0.940
A/Q_F^a	0.6925	0.6925	0.7075
L_{II}/A	0.8100	0.7875	0.7975
L_{III}/A	1.54	1.54	1.56
L_{IV}/A	−0.34	−0.34	−0.35
f_H^{line}	1.3	1.3	1.3
f_X^{line}	1	1	1.1
Feed, wt %			
p-Xylene	18.86	18.93	18.92
m-Xylene	43.03	44.22	44.08
o-Xylene	14.42	13.39	13.86
Ethylbenzene	12.38	10.40	11.99
Nonaromatics	10.83	12.74	10.80
Toluene	0.48	0.32	0.34
Plant surveys	Pumparound Extract out	Pumparound Extract out	Pumparound

process, especially when the number of components and columns is large, as is the case under study.

The particle mass balance for the ith component is[29]

$$\varepsilon_p \frac{\partial \bar{C}_{pij}}{\partial t} + \rho_p \frac{\partial \bar{q}^*_{ij}}{\partial t} = k_i \left(C_{ij} - \bar{C}_{pij}\right) \tag{22}$$

where $\bar{q}^*_{ij}$ (mol/kg of adsorbent) is the average adsorbed concentration of component i in equilibrium with the intraparticle fluid with composition $\bar{C}_{pij}$, ε_p is the particle porosity, and ρ_p (kg/m^3) is the apparent density of the zeolite pellets.

The initial and boundary conditions are, respectively

$$C_{ij} = C^{(0)}_{ij}, \quad \bar{C}_{pij} = \bar{C}^{(0)}_{pij} \quad \text{for} \quad t = 0 \tag{23}$$

$$\begin{cases} z = 0 : \left(u_j\ C_{ij}\right)_{in} = u_j\ C_{ij} - D_{ax} \dfrac{\partial C_{ij}}{\partial z} \\ z = L_j \quad : \quad \dfrac{\partial C_{ij}}{\partial z} = 0 \end{cases} \qquad \forall t > 0 \tag{24}$$

The adsorption equilibrium is described by a multicomponent Langmuir-type isotherm[27]

$$q^*_{ij} = \frac{q_{mi}\ K_i\ C_{pij}}{1 + \sum_{i=1}^{NC} K_i\ C_{pij}} \tag{25}$$

where the K_i (m^3/mol) are the Langmuir constants and the q_{mi} the saturation capacities expressed in mol/(kg of adsorbent).

Node balances

The inlet/outlet nodes are assigned to the ports located between the beds, which are numbered sequentially (Figure 2) and where the fluid is injected/removed to/from the adsorbent chambers by means of the internal piping. The periodic switching of the ports makes the node balances change their position at each switching interval; this means that the location of the different ports must be tracked along the 24 steps of the cycle.

Table 4. Plant Operation Data for the Three Cases of Table 2

Case	A	B	C
A	64.36	80.45	67.92
W	320.68	400.84	338.39
Q_I	481.59	599.71	504.59
Q_{IIA}	382.19	476.08	402.47
Q_{II}	372.80	464.34	392.56
Q_{IIB}	365.57	455.31	384.93
Q_{III}	419.78	524.90	444.34
Q_{IIIA}	429.17	536.64	454.25
Q_{IV}	298.78	373.60	314.62
Q_F	99.40	123.63	102.13
Q_D	130.39	163.04	139.63
Q_X	7.22	9.03	8.39
Q_H	9.39	11.74	9.91
Q_E	54.21	69.59	60.17
Q_R	182.81	226.11	189.97
t^*	112.1	89.7	106.3

The flow rates are expressed in m^3/h and the switch times in s.

The mass balances at the nodes are given by Eqs. 26–39, where "in" and "out" refer to the inlet and outlet positions of a given column j of the SMB unit, respectively. In these equations, Q_k (k=I, II, IIB, IIA, III, IIIA or IV) is the volumetric flow rate in a specific zone of the SMB unit

$$\text{Feed node, F}: Q_F + Q_{IIA} = Q_I \tag{26}$$

$$Q_F C_{i,F} + Q_{IIA} C^{out}_{i,j} = Q_I C^{in}_{i,j+1} \tag{27}$$

$$\text{Raffinate node, R}: Q_I = Q_R + Q_{IV} \tag{28}$$

$$C^{out}_{i,j} = C_{i,R} = C^{in}_{i,j+1} \tag{29}$$

$$\text{Desorbent node, D}: \quad Q_D + Q_{IV} = Q_{IIIA} \tag{30}$$

$$Q_D C_{i,D} + Q_{IV} C^{out}_{i,j} = Q_{IIIA} C^{in}_{i,j+1} \tag{31}$$

$$\text{Flush-out node, Ho}: \quad Q_{IIIA} = Q_{H_o} + Q_{III} \tag{32}$$

$$C^{out}_{i,j} = C_{i,H_o} = C^{in}_{i,j+1} \tag{33}$$

$$\text{Extract node, } E: \quad Q_{III} = Q_E + Q_{IIB} \tag{34}$$

$$C^{out}_{i,j} = C_{i,E} = C^{in}_{i,j+1} \tag{35}$$

$$\text{Recycle node, R}: Q_X + Q_{IIB} = Q_{II} \tag{36}$$

$$Q_X C_{i,X} + Q_{IIB} C^{out}_{i,j} = Q_{II} C^{in}_{i,j+1} \tag{37}$$

$$\text{Flush-in node, Hi}: \quad Q_{H_i} + Q_{II} = Q_{IIA} \tag{38}$$

$$Q_{Fi} C_{i,H_i} + Q_{II} C^{out}_{i,j} = Q_{IIA} C^{in}_{i,j+1} \tag{39}$$

Submodels for the dead-volumes

Three major types of dead volumes exist in the Parex unit: bed lines, circulation lines, and bed-head dead volumes (volume created by the internals).

Bed Lines. As already discussed, the bed lines are the tubing that transfers the fluid between the adsorbent chambers and the rotary valve. These lines represent dead volume

Table 3. Properties for the Nonaromatic Fraction of the Parex Feed Stream

MW (g/mol)	ρ at 177°C (kg/m^3)	η at 177°C (cP)	V_m at 25°C (cm^3/mol)	V_m at 177°C (cm^3/mol)
112.8	604.0	0.1439	150.9	186.8

Table 5. Mass-Transfer Coefficients, Sorption Data, and Péclet Numbers

	k (s^{-1})	K (m^3/mol)	q_m (mol/kg)
p-Xylene	0.08	0.2953	1.256
m-Xylene	0.08	0.0208	1.202
o-Xylene	0.08	0.0255	1.224
Ethylbenzene	0.08	0.0387	1.181
p-Diethylbenzene	0.07	0.8601	0.703
Nonaromatics	0.07	0	0
Toluene	0.08	0.1912	1.213
Pe	1000	Pe_{dead}	200

associated to the SMB unit and are described with a dispersed plug-flow model. The description of the rate of spreading of the cross-sectional average solute concentration, C_i, is written as

$$\frac{\partial C_i}{\partial t}+u_{dead}\frac{\partial C_i}{\partial z}=D_{ax-dead}\frac{\partial^2 C_i}{\partial z^2} \tag{40}$$

where u_{dead} (m/s) is the fluid velocity ($u_{dead}=Q_k/A$, k=I, II, IIB, IIA, III, IIIA or IV) and $D_{ax-dead}$ (m^2/s) is the axial dispersion coefficient in the tube

$$Pe_{dead}=\frac{u_{dead}\ L_{tube}}{D_{ax-dead}} \tag{41}$$

In Eq. 41, L_{tube} (m) is the length of the tube and Pe_{dead} is the Péclet number that measures the extent of axial dispersion in the tubing.

The necessary initial and boundary conditions are, respectively

$$C_i=C_i^{(0)}\ \text{ for }\ t=0 \tag{42}$$

$$\begin{cases} z=0, (u_{dead}\ C_i)_{in}=\ u_{dead}\ C_i-D_{ax-dead}\dfrac{\partial C_i}{\partial z} \\ z=L_{tube},\quad \dfrac{\partial C_i}{\partial z}=0 \end{cases} \quad \forall t>0 \tag{43}$$

As the bed lines are used to inject and remove the streams from the adsorbent beds and they are not used in all steps of the cycle, three cases are possible for the fluid flow: (1) the fluid is injected into the adsorbent chamber ($u>0$); (2) the bed line is not used during a step of the cycle ($u=0$); and (3) the fluid is withdrawn from the adsorbent chamber ($u<0$).

Circulation Lines. The circulation lines are the piping used to transfer the fluid between the bottom of an adsorbent chamber and the top of the other (Figure 1); they are described by Eqs. 40–43. The Parex unit comprises two circulation lines: the PA line and the pusharound line. The flow rate in the PA (circulation line between beds 24 and 1) is imposed by a pump and a valve that regulate the flow rate according to the zone passing through the PA at a given instant. The valve position is determined by Eqs. 11–17, that is, the flow rates imposed are Q_k, k=I, II, IIB, IIA, III, IIIA, and IV. The zone passing through the PA at a specific time step of the cycle is determined from the position of each inlet/outlet stream.

The positions of the streams, P_z (z=E, X, H_i, F, R, D or H_o), in each step of the cycle, $step_{cycle}$ ($1 \le step_{cycle} \le \sum_{k=I,...,IV} N_k$), are defined by Eqs. 44–51, where the number of columns in each zone is given by N_k (k=I, II, IIB, IIA, III, IIIA or IV) and $P_E^{(0)}$ is the initial position of the extract port (used to define the starting point of the cycle)

$$\text{Extract port}: \ P_E^{'}=step_{cycle}+P_E^{(0)} \tag{44}$$

$$\text{Recycle port}: \ P_R^{'}=step_{cycle}+P_E^{(0)}+N_{IIB} \tag{45}$$

$$\text{Flush-in port}: P_{H_i}^{'}=step_{cycle}+P_E^{(0)}+N_{IIB}\ +\ N_{II} \tag{46}$$

$$\text{Feed port}: \ P_F^{'}=step_{cycle}+P_E^{(0)}+N_{IIB}\ +\ N_{II}\ +N_{IIA} \tag{47}$$

$$\text{Raffinate port}: P_R^{'}=step_{cycle}+P_E^{(0)}+N_{IIB}\ +\ N_{II}\ +N_{IIA}\ +N_I \tag{48}$$

$$\text{Desorbent port}: \ P_D^{'}=step_{cycle}+P_E^{(0)}+N_{IIB}\ +\ N_{II}\ +N_{IIA}\ +N_I\ +N_{IV} \tag{49}$$

$$\text{Flush-out port}: P_{H_o}^{'}=step_{cycle}+P_E^{(0)}+N_{IIB}\ +\ N_{II}\ +N_{IIA}\ +N_I\ +N_{IV}\ +N_{IIIA} \tag{50}$$

$$P_z=\begin{cases} P_z^{'}, & P_z^{'}\le \sum_{k=I,...,IV} N_k \\ P_z^{'}-\sum_{k=I,...,IV} N_k\ , & P_z^{'}>\sum_{k=I,...,IV} N_k \end{cases} \tag{51}$$

z=E, X, H_i, F, R, D or H_o

Once the position P_z of each stream is known, the flow rate imposed at the outlet of the PA line is determined by knowing the stream with the highest position in the train of beds/nodes:

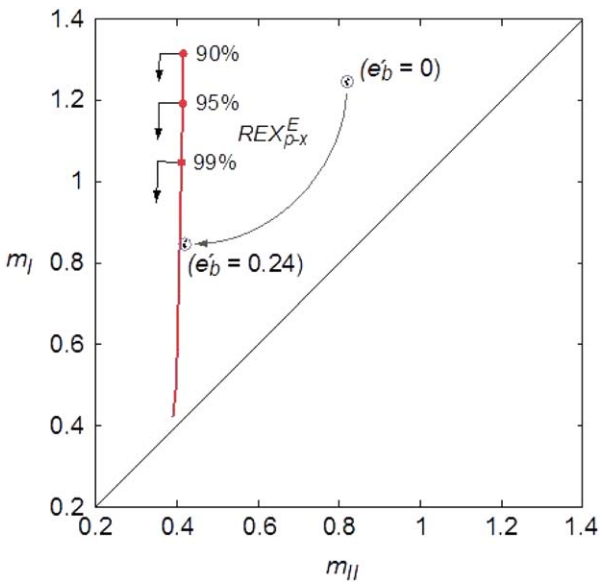

Figure 4. Operating line on the $m_{II}\times m_I$ plane of the Parex's TMB analog for PUX^E_{p-x}=99.7% and $REX^E_{p-x} \ge$ 90, 95, and 99%.

The symbols represent the working values of $\{m_I, m_{II}\}$ for the three industrial Cases A, B, and C (c.f. Tables 2 and 4) determined from Table 4 using the conversion rules given in Eq. 62 with (ε'_b=0.24) and without (ε'_b=0) the correction for the presence of dead volumes. [Color figure can be viewed in the online issue, which is available at wileyonlinelibrary.com.]

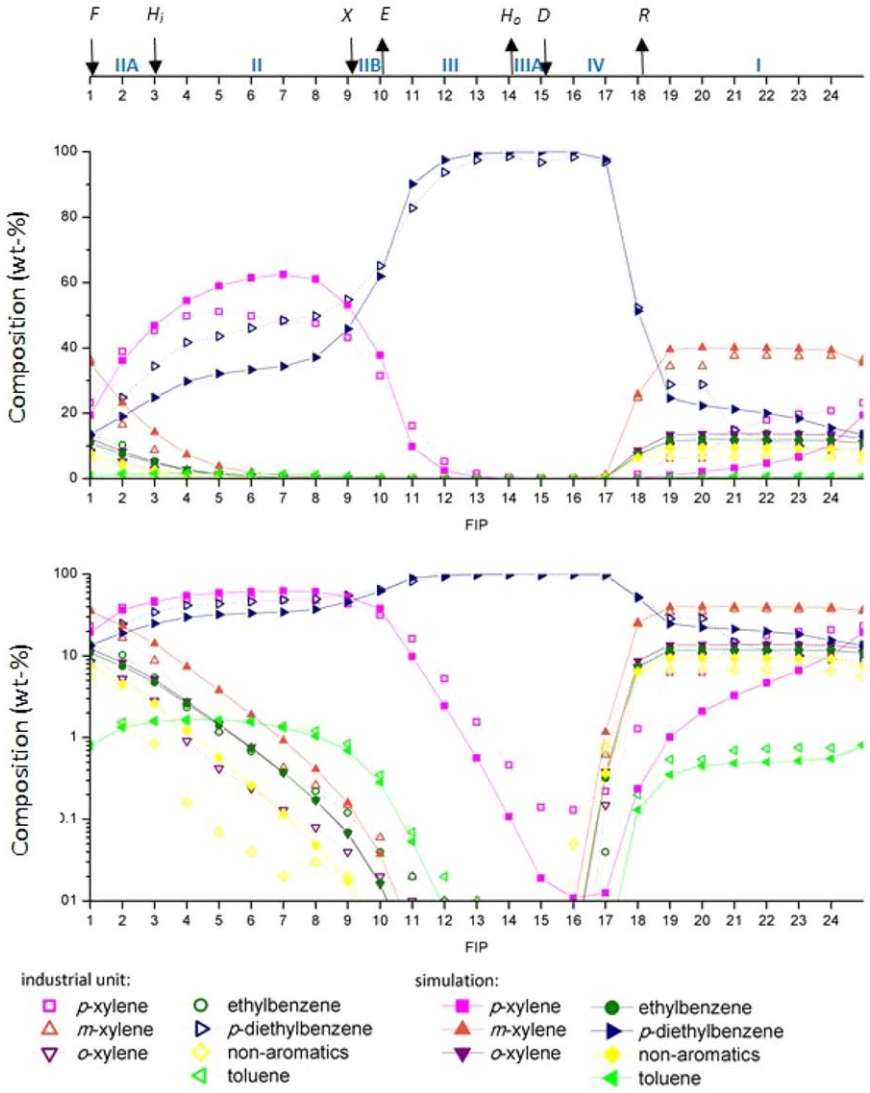

Figure 5. Experimental concentration profiles (wt %) measured in the PA line and simulation results as a function of the FIP for industrial case study A.

[Color figure can be viewed in the online issue, which is available at wileyonlinelibrary.com.]

$$Q_{\text{pumparound}} = \begin{cases} Q_{\text{I}}, & \max_z P_z = P_{\text{F}} \\ Q_{\text{II}}, & \max_z P_z = P_{\text{X}} \\ Q_{\text{IIA}}, & \max_z P_z = P_{\text{H}_i} \\ Q_{\text{IIB}}, & \max_z P_z = P_{\text{E}} \\ Q_{\text{III}}, & \max_z P_z = P_{\text{H}_o} \\ Q_{\text{IIIA}}, & \max_z P_z = P_{\text{D}} \\ Q_{\text{IV}}, & \max_z P_z = P_{\text{R}} \end{cases} \tag{52}$$

Bed-head dead volume. The liquid flow through the bed-head dead volume is modeled as a continuous stirred tank, that is, $VdC_i/dt = F(C_i^{\text{in}} - C_i)$ with $C_i = C_i^{(0)}$ for $t = 0$.

Model Implementation and Numerical Solution

The implementation of the model can be understood by considering different submodels as building blocks connected to each other through different connection types, which can be carriers of any type of information (e.g., stream parameters).

In the SMB model, 24 fixed-bed submodels, preceded by bed-head dead volume submodels, are interspersed by node balances. A bed line submodel is connected to each node (Figure 2). Four hypothetical blocks, where the information about the streams is contained, are created. For the feed and desorbent streams, concentrations and flow rates are defined as input parameters. For the extract and raffinate streams, only the flow rates are defined as input parameters. These building blocks where information is input are connected to all bed lines by means of hypothetical on–off valves (which control the passage of information). The bed lines have flow of information in both directions and its direction is controlled by the opening and closing of hypothetical on–off valves placed at both ends of the bed lines. These valves stop the flow inside the bed lines and hold the information as it happens in the Parex unit.

To simulate the periodic switching of the ports, starting from an initial position, the valves are opened or closed

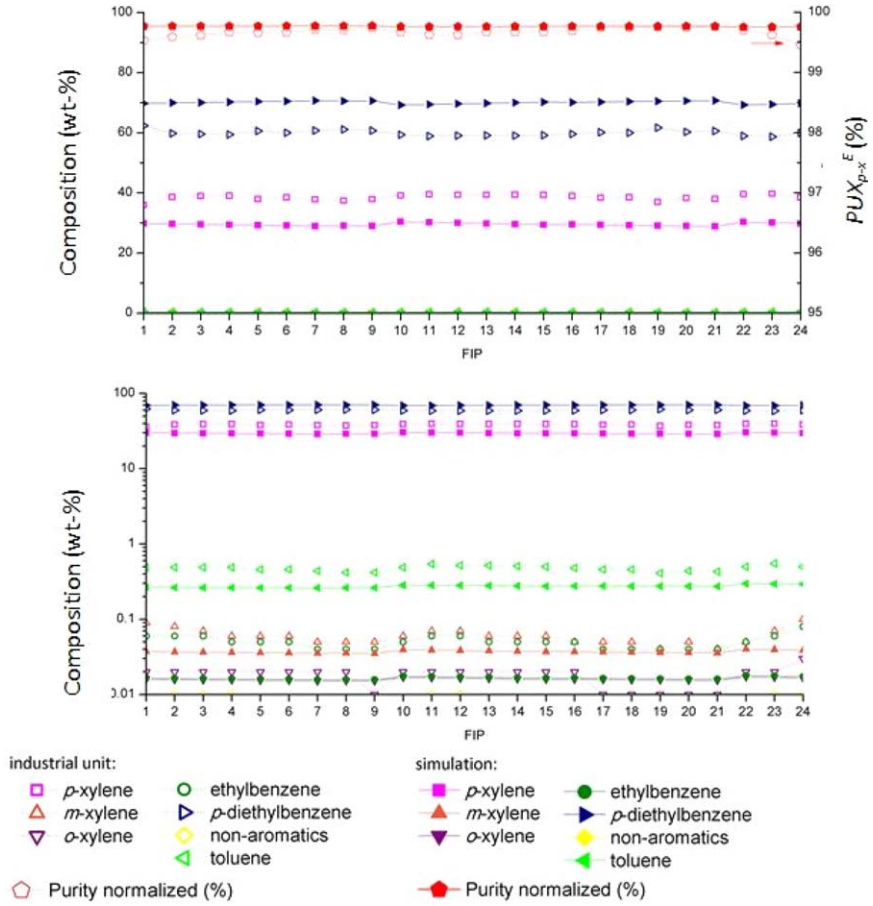

Figure 6. Experimental data and simulation results of the extract composition (wt %) as a function of the FIP for industrial case study A.

[Color figure can be viewed in the online issue, which is available at wileyonlinelibrary.com.]

sequentially according to the configuration of the SMB unit, that is, according to the number of beds per zone.

Besides the feed, desorbent, extract, and raffinate, three more streams are considered: flush in, flush out, and secondary flush (recycle). The secondary flush is a split from the main desorbent stream and, therefore, they both have the same composition. The flush-out stream is withdrawn at one predefined port and bed line, and is immediately injected into the bed line corresponding to the flush-in position. If this model is simplified to a four-zone SMB model, the wash percentage of the primary flush and secondary flush, as well as the length of the bed lines, can be set to zero.

For completeness, it is worth noting that there is an alternative approach for simulating the rotary valve if there were no dead volumes in the PA and pusharound circulation lines. In this alternative approach, the positions of the inlet and outlet ports of the rotary valve are fixed and are not switched at the end of a switching interval; instead, the axial concentration profiles for each column and for its bed-head dead volume at the end of a switching interval become the initial concentration profiles for the downstream column at the beginning of the next switching interval. This makes the model easier to implement because the node balances, as well as the inlet and outlet streams, are fixed to specific columns. This approach, however, is only applicable when every column goes exactly through the same set of steps. Because in the Parex unit the PA and pusharound lines are connected to specific columns, the cycle is not exactly t^*-periodic; it is approximately t^*-periodic and exactly Nt^*-periodic (N represents the number of columns).

The model was implemented in gPROMS version 3.3.1. (Process System Enterprise, London, UK); the PDAEs system was reduced to a system of ordinary differential and algebraic equations in time by discretization of the axial domains using third-order orthogonal collocation on finite elements. The resulting system of sparse ordinary differential equations was integrated in time by the gPROMS solver DASOLV with a relative error tolerance of 10^{-5}.

The fixed-bed submodel was discretized with one finite element per 80 theoretical plates (TPs). In the Parex unit, the maximum number of TPs per column is obtained for *p*-diethylbenzene, $NTP_{\max} = 400$; for *p*-xylene the number is slightly smaller, NTP = 357; this gives five uniform finite elements per column and 120 elements in total. The bed lines and circulation lines were discretized into 21 and 37 uniform finite elements, respectively. The adopted grid resolution is the result of preliminary tests with the model and provides a good compromise between accuracy and computational overhead.

In the dynamic simulations of the Parex unit, it was assumed that the cyclic steady state (CSS) was achieved after five complete cycles when the balance error (%)

$$\text{balance error} = 100 \times \sum_{i}^{NC} \frac{|Q_F\ C_i^F - \left(Q_E\ \bar{C}_i^E + Q_R\ \bar{C}_i^R\right)|}{Q_F\ C_i^F} \qquad (53)$$

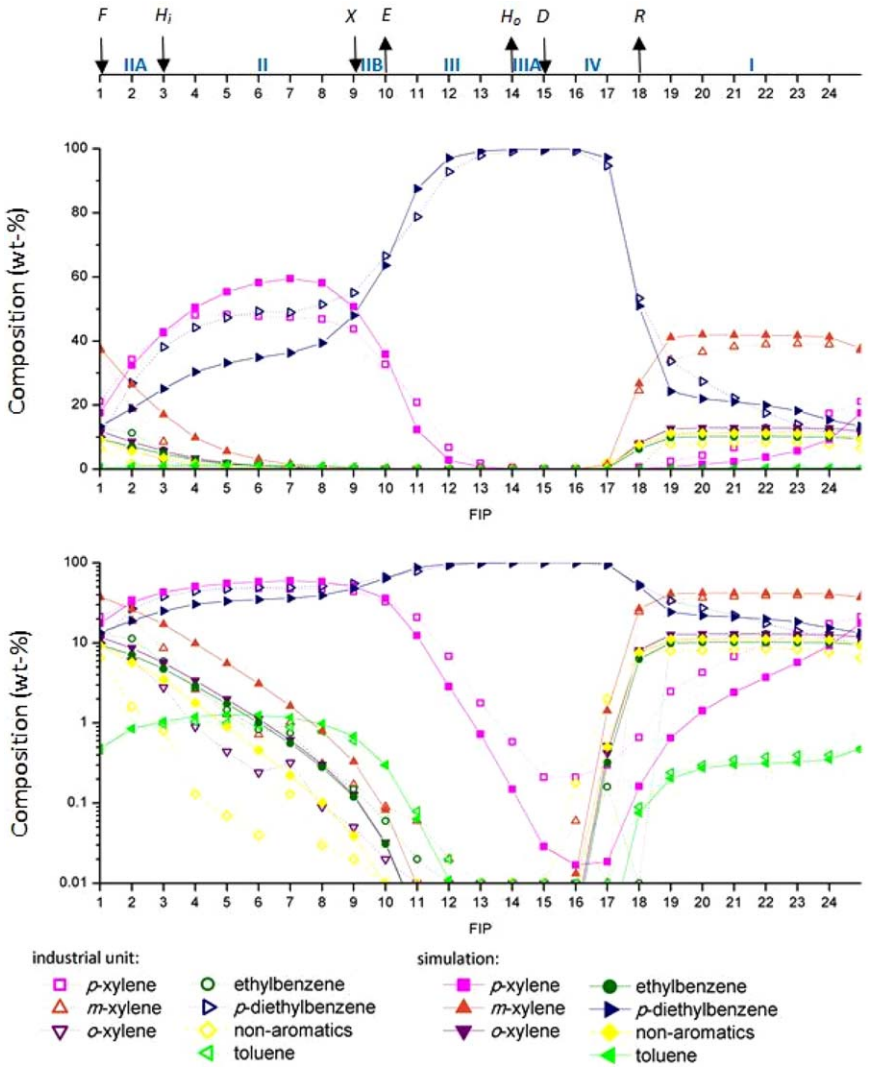

Figure 7. Experimental concentration profiles (wt %) measured in the PA line and simulation results as a function of the FIP for industrial case study B.

[Color figure can be viewed in the online issue, which is available at wileyonlinelibrary.com.]

was below 2%. Here, the average concentrations in the extract and raffinate streams, $\bar{C}_i^{\mathrm{E}}$ and $\bar{C}_i^{\mathrm{R}}$, are calculated over a single switching interval $(n=1)$ or over a full cycle $(n=24)$

$$\bar{C}_i^{\mathrm{E\ (or\ R)}} = \frac{1}{n\ t^*} \int_{t}^{t+n\ t^*} C_i^{\mathrm{E\ (or\ R)}}\ dt \tag{54}$$

and represent the concentrations that would be measured after collecting the fluid into a perfectly mixed cup.

All simulations were performed in a Windows workstation equipped with a 2.5 GHz quad-core Intel processor. It is worth noting that each simulation took a CPU time of about 8 h to complete 17 cycles, which is approximately the number of cycles needed to attain the CSS.

Simulation of an Industrial-Scale Parex Unit

To evaluate the performance of the separation of *p*-xylene in the Parex unit, four performance parameters are considered: purity (wt %), PUX; recovery (wt %), REX; desorbent consumption (kg of *p*-diethylbenzene per kg of *p*-xylene obtained in the extract), DC; and productivity (kg of *p*-xylene obtained in the extract per hour and per cubic meter of adsorbent), PR

$$\mathrm{PUX}_{p-\mathrm{x}}^{\mathrm{E}} = 100 \frac{\bar{C}_{p-\mathrm{x}}^{\mathrm{E}}}{\sum_i \bar{C}_i^{\mathrm{E}} - \bar{C}_{p-\mathrm{DEB}}^{\mathrm{E}}} \tag{55}$$

$$\mathrm{REX}_{p-\mathrm{x}}^{\mathrm{E}} = 100 \frac{Q_{\mathrm{E}}\ \bar{C}_{p-\mathrm{x}}^{\mathrm{E}}}{Q_{\mathrm{F}}\ C_{p-\mathrm{x}}^{\mathrm{F}}} \tag{56}$$

$$\mathrm{DC} = \frac{Q_{\mathrm{D}}\ C_{p-\mathrm{DEB}}^{\mathrm{D}}}{Q_{\mathrm{E}}\ \bar{C}_{p-\mathrm{x}}^{\mathrm{E}}} \tag{57}$$

$$\mathrm{PR} = \frac{Q_{\mathrm{E}}\ \bar{C}_{p-\mathrm{x}}^{\mathrm{E}}}{V_{\mathrm{solid}}} = \frac{Q_{\mathrm{E}}\ \bar{C}_{p-\mathrm{x}}^{\mathrm{E}}}{24\ (1-\varepsilon_b)\ V_{\mathrm{c}}} \tag{58}$$

In these equations, the concentrations in the extract stream are averages over a switching interval, t^*, as in Eq. 54 and expressed in kg/m^3.

In the Parex process, the purity goal is 99.7 wt % of *p*-xylene in the extract stream and the recovery should be as high as possible within the purity specification. Usually, the purity values of the extract stream are normalized, that is,

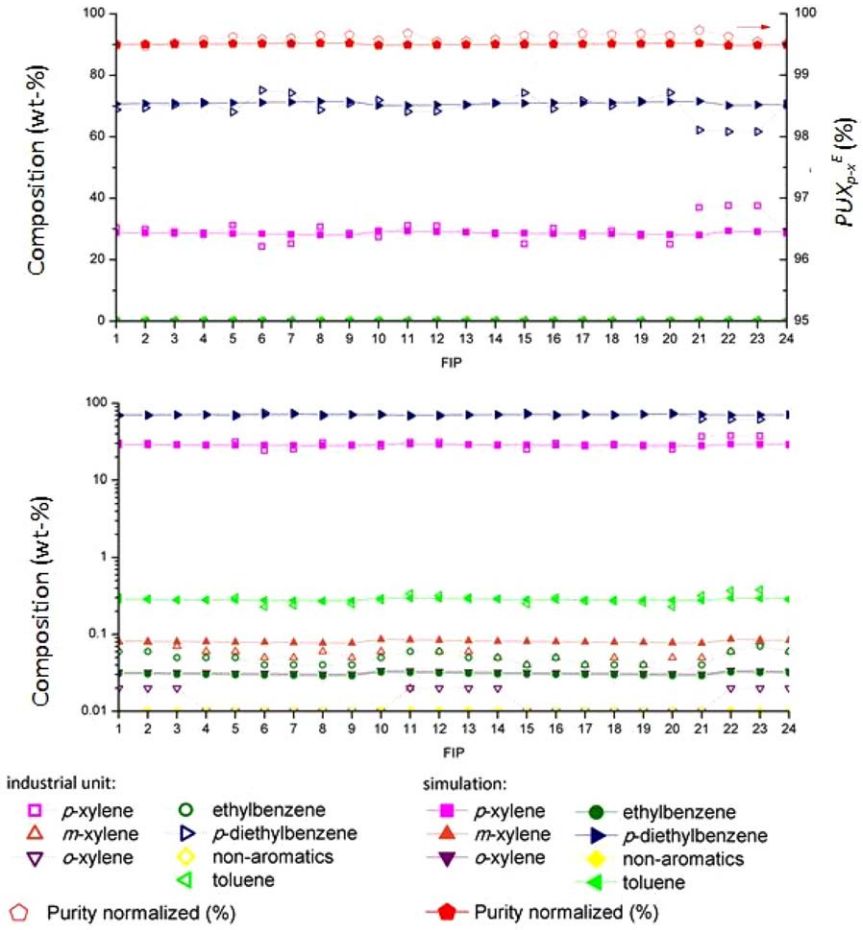

Figure 8. Experimental data and simulation results of the extract survey (wt %) as a function of the FIP for industrial case study B.

[Color figure can be viewed in the online issue, which is available at wileyonlinelibrary.com.]

only *m*-xylene, *o*-xylene and ethylbenzene are considered as impurities. Before storage, *p*-xylene is sent at 145°C to a finishing column where the C_7 components (b.p. 110.6°C for toluene) and other impurities with low boiling points (nonaromatic fraction defined with C_8 naphthenic components with b.p. between 104 and 132°C) are separated through the top of the column.

Three sets of industrial data (PA and extract surveys)—Cases A, B, and C—were compared with the SMB simulations. Table 2 defines the operating parameters for the three case studies. The necessary data in terms of adsorbent and unit design for simulating these three cases are given in Table 1. Given that the three sets of data were obtained from the same industrial unit, it is understandable that they do not deviate significantly from each other. In fact, $Q_F\tau^*$ does not deviate more than 1.5% and $Q_D\tau^*$ more than 1%; as $1/\tau^*$ is directly proportional to the volumetric solid flow rate, Q_s, of the equivalent TMB unit, it is thus concluded that the ratios Q_j/Q_s were kept constant at the industrial plant. The cases of academic interest in which the plant is operated far outside of the specifications are very difficult to find and even harder to disclose.

To simulate the operation of the SMB unit, the nonaromatic fraction must be characterized. It is assumed that the composition of this faction has the same properties as the C_8 nonaromatic fraction in the effluent of the xylene isomerization reactor described by Neuzil.[49] The thermodynamic and transport properties, needed by the gPROMS simulations, were determined using the commercial software Aspen Hysys version 2006.5 (Aspen Technology, MA). Table 3 gives the

Table 6. Comparison Between the Performance of the Industrial Unit and the Simulation Results

Case	PUX_{p-x}^{E} (wt %)	REX_{p-x}^{E} (wt %)	DC (kg/kg)	PR (kg h^{-1} m^{-3})
A				
Plant	99.70	83.00	–	–
PA survey	99.64	81.65	8.76	56.75
EO survey	99.67	112.78	6.34	78.39
Simulation	99.76	97.64	7.33	67.87
B				
Plant	99.70	92.20	–	–
PA survey	99.52	89.02	8.08	76.99
EO survey	99.60	96.40	7.46	83.34
Simulation	99.53	97.70	7.36	84.49
C				
Plant	99.71	93.25	–	–
PA survey	99.57	89.12	8.34	63.84
EO survey	–	–	–	–
Simulation	99.64	97.69	7.61	69.98

Normalized purity, PUX_{p-x}^{E} (wt %); recovery, REX_{p-x}^{E} (wt %); desorbent consumption, DC (kg of *p*-diethylbenzene per kg of *p*-xylene obtained in the extract); and productivity, PR (kg of *p*-xylene obtained in the extract per hour per cubic meter of adsorbent).
Surveys: PA, Pumparound; EO, Extract out.

Table 7. Simulation Results of Purity and Recovery for Case C: Base Case, 10% Loss, and 20% Loss in Adsorbent Capacity

Capacity Loss (%)	PUX^{E}_{p-x} (%)	REX^{E}_{p-x} (%)
0	99.64	97.69
10	99.67	94.67
20	99.68	88.43

relevant thermodynamic and transport properties of the nonaromatic fraction of the Parex feed stream.

It is important to note that during operation of the unit, the aromatic fraction in the feed in not always adjusted for the calculation of the operating flow rates (Table 2). Usually an average value is considered. In all simulations, it was considered that the desorbent is pure *p*-diethylbenzene.

Table 4 lists the plant operation input values obtained by applying Eqs. 3–20 to the operating parameters given in Table 2.

Table 5 gives the mass-transfer coefficients and Langmuir adsorption isotherm parameters,[27] as well as the Péclet numbers for the beds and dead volumes (bed and circulation lines).

It is of interest to first analyze the results in the framework of reduced-order modeling, such as the equilibrium theory or TMB analogy. Because of the Parex's finite column efficiency, we resort to the TMB approach instead of the equilibrium theory.

The steady-state TMB analog of the CSS SMB model can be written as

$$(1-\varepsilon_b)k_i\left(C_{ij}-\bar{C}_{pij}\right)=\frac{Q_j^{TMB}}{V_j}\left(\frac{1}{Pe}\frac{\partial^2 C_{ij}}{\partial x^2}-\frac{\partial C_{ij}}{\partial z}\right) \tag{59}$$

$$(1-\varepsilon_b)k_i\left(\bar{C}_{pij}-C_{ij}\right)=\frac{Q_s}{V_j}\frac{\partial}{\partial x}\left(\varepsilon_p\bar{C}_{pij}+\rho_p\bar{q}^*_{ij}\right) \tag{60}$$

where i is the component index and j the zone index; x is the dimensionless coordinate along the length of zone j, $V_j = n_j V_c$ the volume of the zone, n_j the number of columns in the zone, and V_c the volume of an SMB column; Q_j^{TMB} is the volumetric flow rate of fluid in zone j and Q_s the volumetric flow rate of the countercurrent moving solid.

The equivalence rules between the TMB and SMB models are[11]

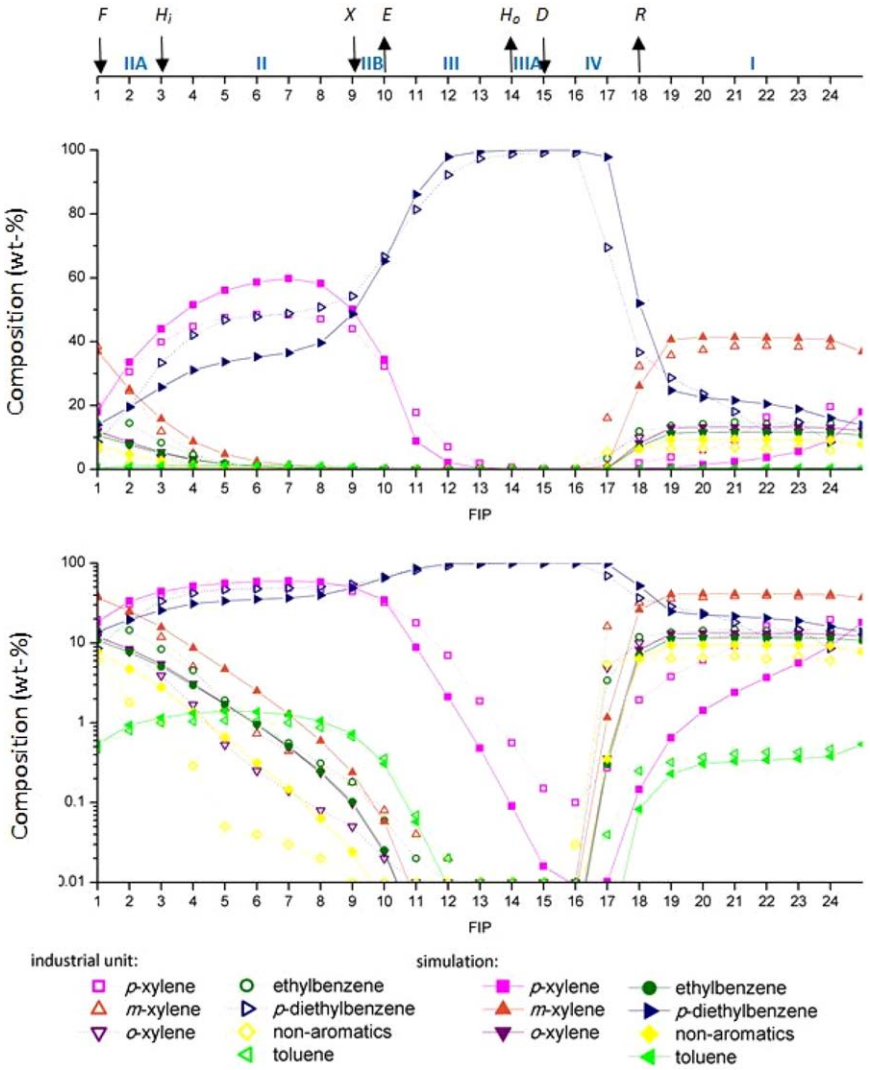

Figure 9. Experimental data and simulation results of the concentration profiles (wt %) measured in the PA line as a function of the FIP for industrial case study C.

[Color figure can be viewed in the online issue, which is available at wileyonlinelibrary.com.]

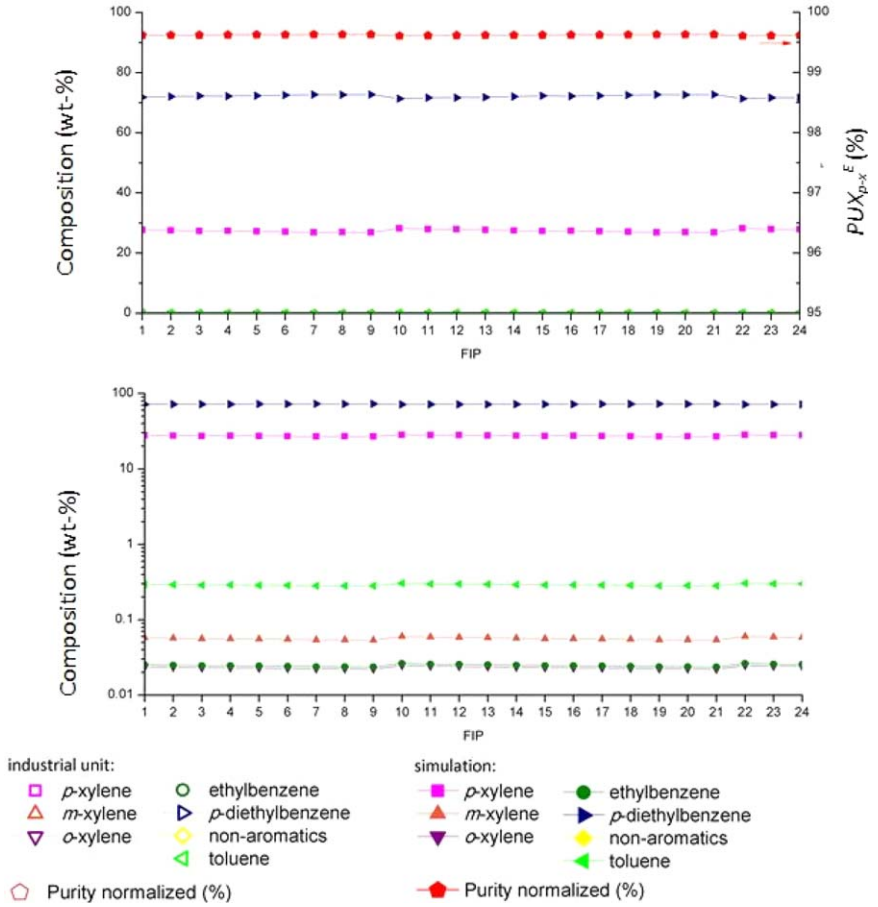

Figure 10. Experimental data and simulation results of the extract survey (wt %) as a function of the FIP for industrial case study C.

[Color figure can be viewed in the online issue, which is available at wileyonlinelibrary.com.]

$$Q_s = \frac{(1-\varepsilon_b)V_c}{\tau^*}, \quad m_j = \frac{Q_j^{TMB}}{Q_s} = \frac{Q_j^{SMB}}{Q_s} - \frac{\varepsilon_b}{1-\varepsilon_b} \tag{61}$$

where the m-parameters represent the ratios of fluid to solid volumetric flow rates.[50–52]

If the SMB unit has non-negligible dead volumes, the TMB model must be modified or the equivalence rules altered. The latter approach is followed here. From the plant specifications (Table 1), the bed-head volumes are the most significant dead volumes in the Parex unit, so these are the ones taken into consideration in the analysis.

Let $\varepsilon_b' = V_{bh}/V_c = 0.22/0.91 = 0.24$ be a measure of the bed-head dead volume with respect to the column volume. Although the volume of solid in zone j is still $(1-\varepsilon_b)V_j$, the volume of interparticle fluid is now $(\varepsilon_b+\varepsilon_b')V_j$. This means that the dead volume does not change the relation between Q_s and τ^*, but reduces the value of Q_j^{TMB} because a larger flow rate is needed to displace the extra interparticle fluid during the switching interval τ^*. Thus, although in Eq. 61, a non-zero value of ε_b' does not affect the term $1-\varepsilon_b$ in the denominator of the conversion rule, because it measures the volume of solid, ε_b in the numerator should be replaced by $\varepsilon_b+\varepsilon_b'$ to account for the extra fluid in the dead volume. Hence, the corrected equivalence rules should be

$$Q_s = \frac{(1-\varepsilon_b)V_c}{\tau^*}, \quad m_j = \frac{Q_j^{TMB}}{Q_s} = \frac{Q_j^{SMB}}{Q_s} - \frac{\varepsilon_b+\varepsilon_b'}{1-\varepsilon_b} \tag{62}$$

The four-zone TMB analog of the SMB model of the Parex unit (I-II-III-IV = 7-9-5-3) was solved subject to the constraints $PUX_{p-x}^E = 99.7\%$ and $REX_{p-x}^E \geq REX_{min}$ for $REX_{min} = 90$, 95, and 99%. In line with the SMB simulations, PUX_{p-x}^E is a normalized value, that is, only m-xylene, o-xylene, and ethylbenzene are considered as impurities. The discussion is focused on the usual $m_{II} \times m_I$ plane of the two central separation zones.

The value of Q_s was determined from the mean value of the switching intervals of the three industrial case studies (Table 4) and kept fixed. First, the m-difference $m_I - m_{II} \propto Q_F$ was maximized subject to $PUX_{p-x}^E = 99.7\%$ and $REX_{p-x}^E \geq REX_{min}$ to determine the maximum working value $m_F^{max} = m_I - m_{II}$ for a given REX_{min}. Then, $m_I - m_{II}$ was progressively relaxed, say $m_I - m_{II} \geq m_F^{min}$ with $m_F^{min} < m_F^{max}$, and the m-difference $m_{III} - m_{IV} \propto Q_D$ was minimized to determine the minimal desorbent requirement for each relaxation. Figure 4 shows a representation on the $m_{II} \times m_I$ plane of the results obtained for $REX_{min} = 90$, 95, and 99%. The data lie on a single curve that extends toward larger m_I values as the recovery requirement is set to a less stringent specification

It is of interest to determine how far off from the TMB line lie the working (m_I, m_{II}) values of the three industrial cases. A blunt analysis neglecting the Parex's bed-head dead volumes ($\varepsilon_b' = 0$) places the industrial operating points quite far from the TMB operating line. However, if the $\{m_I, m_{II}\}$ values are corrected for the presence of the dead volumes

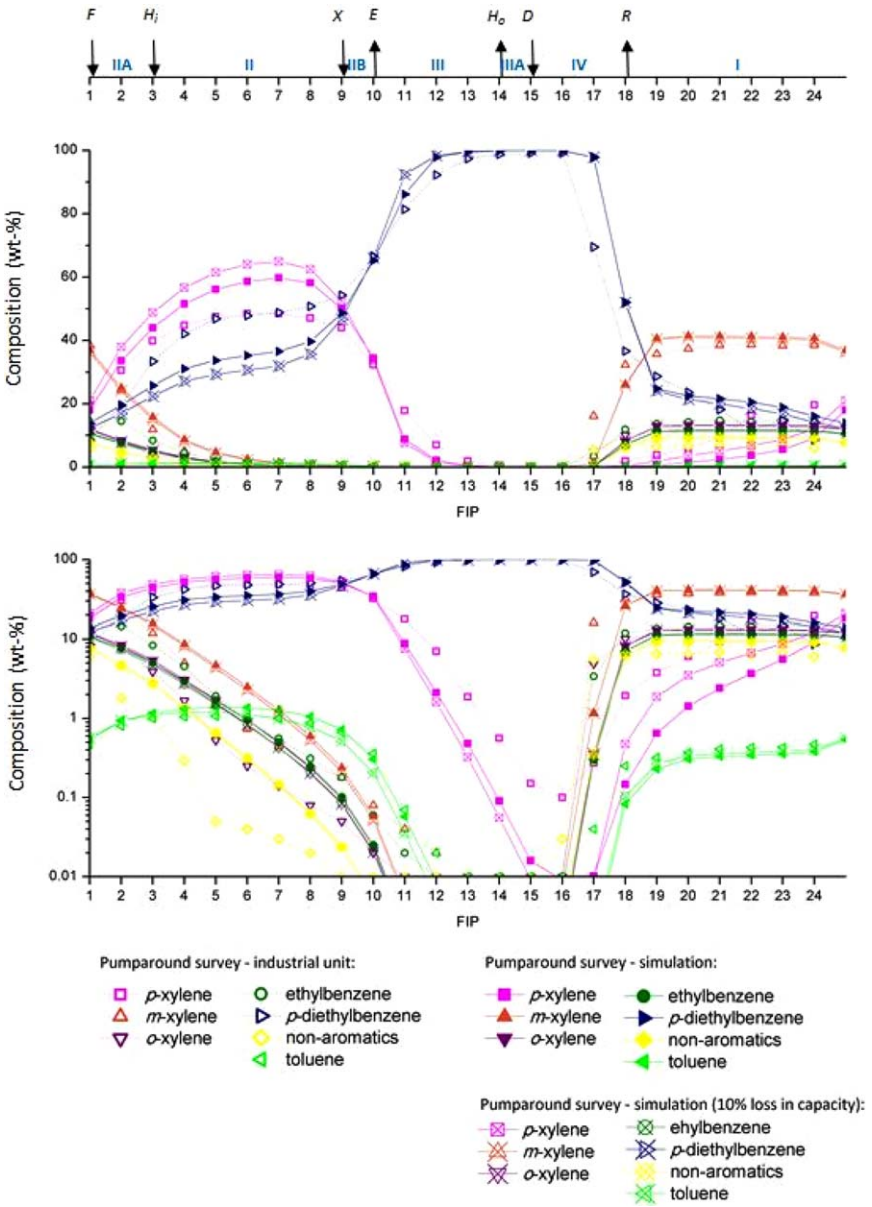

Figure 11. Composition profiles (wt %) measured in the PA line as a function of the FIP for Case C: industrial data and simulation results considering a 10% loss in capacity.

[Color figure can be viewed in the online issue, which is available at wileyonlinelibrary.com.]

($\varepsilon_b'=0.24$) by means of Eq. 62, it is seen that the industrial operating points lie very close to the optimal TMB line. Moreover, the m_I values are well below the upper boundary for $REX^E_{p-x} \geq 99\%$, which explains why the industrial unit was operating correctly.

Figures 5–10 show the detailed SMB simulation results for the three case studies and their comparison with the available data from the plant (Table 2). The concentration profiles in the PA line are plotted as a function of the FIP, which allows the comparison of concentration profiles between cases taken at different switching intervals.

The purity values shown in Figures 6, 8, and 10 are normalized values, that is, in Eq. 56 the i index in the summation runs over p-xylene, m-xylene, o-xylene, and ethylbenzene. The presence of toluene and nonaromatics is neglected in this calculation as these components are easily removed from the extract stream in the finishing column located downstream of the process. An analysis of the mass balance in the finishing column shows that toluene and nonaromatics in the final product never exceed 5% of the amount in the extract stream at the outlet of the Parex unit. In terms of absolute values, these impurities are almost vestigial in the final product (e.g., for Case C, they are less than 0.05% of the stream).

The results of the simulations are summarized in Table 6 and compared with the average performance descriptors (purity and recovery) determined in the plant on the day of the (PA) and/or extract-out (EO) surveys. Table 6 also includes the performance results calculated from the EO or PA survey data. The calculation of the performance descriptors from the extract surveys is based on the averaged values obtained over a cycle. For the calculation of concentrations in the extract from the PA survey data, it is necessary to understand how the concentration varies in the extract stream during a switching interval

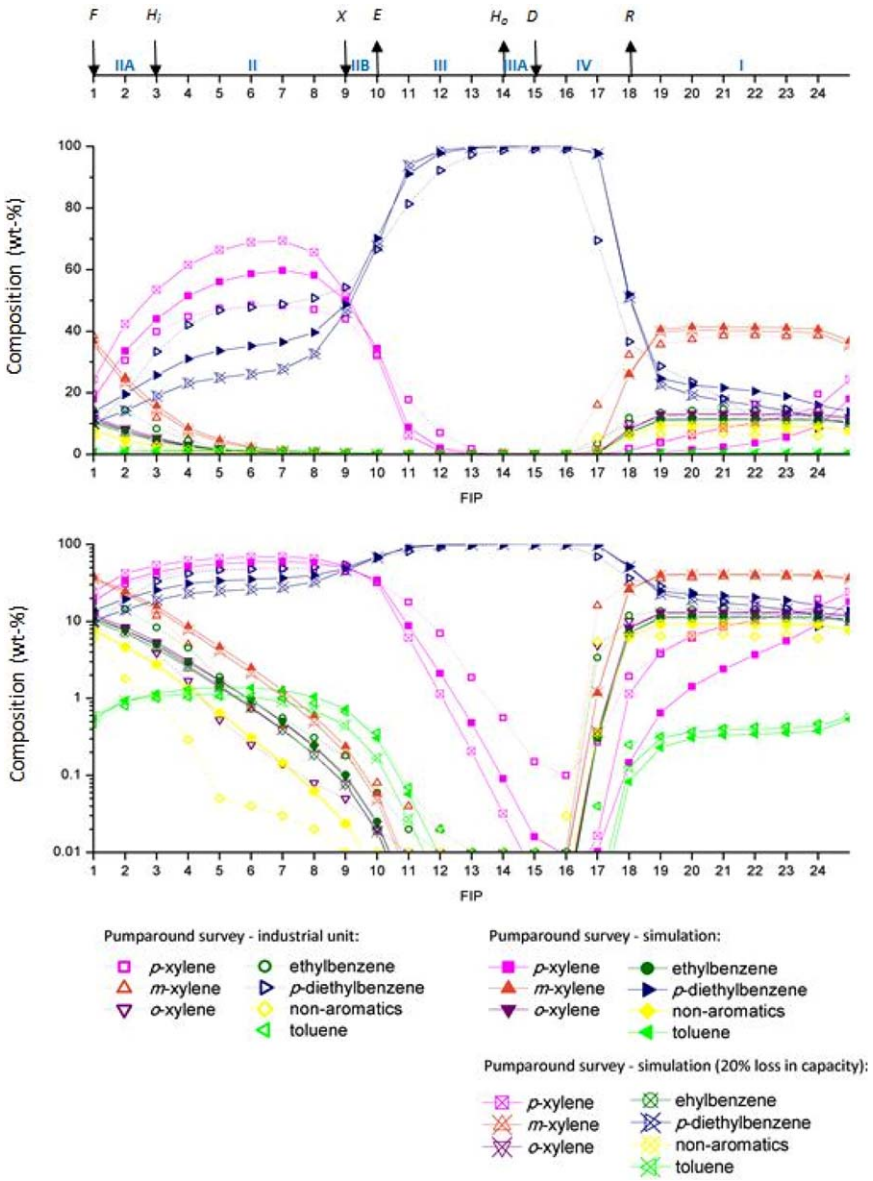

Figure 12. Composition profiles (wt %) measured in the PA line as a function of the FIP for Case C: industrial data and simulation results considering a 20% loss in capacity.

[Color figure can be viewed in the online issue, which is available at wileyonlinelibrary.com.]

because the extract concentration is affected by presence of bed lines; this is discussed in detail below.

By observing the PA and extract surveys presented in Figures 5–10, it can be concluded that generally a good fitting between the simulations and the industrial data is observed. Although there are many causes for the imperfect match between simulations and plant data, the major one is the reasonable, but not perfect, description of the adsorption isotherms. The selective pore volume of the adsorbent packed in the unit is 48.11 m^3, corresponding to a selective void fraction $\varepsilon_\mu = 0.14$, and refers to the adsorbent capacity under a controlled amount of water in the adsorbent. This value is different from the one obtained by us in a previous study of fixed-bed multicomponent breakthroughs of the Parex's feed components,[27] $\varepsilon_\mu = 0.11$, because, among other issues, the experiments were performed under conditions where the amount of water in the adsorbent was not controlled. The mismatch may also be related to a loss in adsorption capacity developed over the years, as discussed in the next section.

Regarding the PA surveys A, B, and C in Zone II ($1 < \text{FIP} < 10$), the simulations predict a higher *p*-xylene concentration than the values measured in the plant, specifically in FIP's between 4 and 9; however, the concentration of this component predicted by the model in the extract point (FIP = 10) is always within a maximum absolute deviation of 8 wt % with respect to the value measured in the plant (1.7, 4.8, and 7.9 wt %, respectively, for Cases A, B, and C).

The analysis Zone II shows that the predicted concentration of *p*-diethylbenzene is lower than the industrial data; however, once again, the differences in the extract point (FIP = 10) are faded. The other xylenes (*m*-xylene, *o*-xylene), which are in small concentrations in this zone, ethylbenzene and the nonaromatic fraction are all above the concentrations measured in the industrial plant; this is seen in detail in the graphs presented in logarithmic scale. Overall, however, these differences are only relevant in the extract position where the concentrations are below 0.1 wt %.

As the time intervals when the samples were collected in the PA surveys are not precisely known, these sampling time intervals might not have been constant during one PA survey or between the PA surveys, and therefore, the comparison with the simulation results may not be coincident. The same applies to the results presented in the extract surveys. In the simulations, the average over a full switching interval was considered.

Zone II should avoid the passage of *m*-xylene, *o*-xylene, ethylbenzene, toluene, and nonaromatics to Zone III. The industrial data show the presence of some of these components in beds 10–13, however, they are only present in very small concentrations and no passage of these components to Zone IV is observed. The simulations show the same behavior up to bed 12.

Even though a good fitting is observed in Zones III and IV, where the adsorbent and desorbent are regenerated, the simulation fails to predict the *p*-xylene concentration below 1 wt %. However, the absolute difference between the simulations and the real data are never higher than 0.12 wt % at the lowest *p*-xylene concentration point (FIP = 16). At the raffinate withdrawal position (FIP = 18), all other components are better fitted than *p*-xylene.

The analysis of the industrial data shows a passage of *p*-xylene between Zones III and I (through Zone IV), which increases the *p*-xylene concentration in the raffinate and, consequently, reduces the recovery of the unit and the conversion in the isomerization reactor (Isomar). In the simulations, the adsorption in Zone III can be considered complete and the passage of *p*-xylene to Zone I is only residual.

Small deviations between the simulations and the plant data are observed in Zone I, especially for *m*-xylene, *o*-xylene, ethylbenzene, and nonaromatics. The deviations between the simulations and the industrial data for toluene are very small in all zones.

The industrial extract surveys (available for Cases A and B) allow a comparison between simulations and the industrial data in the FIP 10 for one complete cycle, that is, the evolution of the purity of the extract during one cycle can be studied. In line with the analysis of the PA surveys, the major deviations in the composition of the extract stream are in the impurities of the extract, that is, in the components below 1 wt %. These differences are reflected in the purity of the extract stream.

The recovery calculated from the average concentrations of the extract in survey A is higher than 100%, suggesting that the analysis of the samples in this case gave values that are too high. In Case A, the recovery calculated from the industrial data for the PA gives a value close to the simulation. Conversely, the recovery values calculated by both methods are consistent in Cases B and C.

The differences in the desorbent consumption and productivity are a consequence of the differences observed in the *p*-xylene concentration in the extract stream.

Simulation of the Parex Unit with Loss of Adsorption Capacity

As observed in Table 6, the mathematical model predicts a recovery that is slightly higher than the results obtained in the plant, which can be related to a loss in adsorption capacity developed over the years ($q_{mi} = q_m^0(1-\xi\ t)$). In this section, the influence of the adsorbent capacity loss on the performance of the unit is studied for Case C.

In Case C, approximately 10 years have passed as the start-up of the unit. Case C was simulated with a loss of capacity of 10% ($\xi = 1\%$/year) and 20% ($\xi = 2\%$/year); the results are shown in Figures 11 and 12. The results show that the capacity loss affects essentially the recovery of the unit (Table 7). Capacity losses of 10 and 20% correspond to recovery losses of 3.0 and 9.2%, respectively.

From the analysis of the concentration curves of *p*-xylene in Figures 9, 11, and 12, it can be concluded that the inclusion in the model of a loss in adsorption capacity brings the simulated *p*-xylene curve closer to the measured one in the plant in Zone I. When the evolution of the *p*-xylene curve in Zone I over the years of operation is analyzed, one can see that the concentration of this component has increased despite the fact that the conditions of operation have not changed significantly.

Conclusions

The design and operation of an industrial-scale, seven-zone SMB unit (configuration: 7-2-6-1-4-1-3) for the separation of *p*-xylene (Parex) was studied in detail. The SMB model with 24 fixed-bed columns considers three types of dead volumes: the bed lines connecting the rotary valve to the 24 ports of the adsorbent chambers, the two circulation lines connecting beds 12–13 (pusharound line) and 24 to 1 (PA line), and the dead volumes created by the internals located before each fixed-bed column.

The model was successfully tested against three groups of data collected in the plant, namely, extract and PA surveys. The comparison between the industrial data and the simulation results shows that the model is capable of predicting the performance of the industrial unit.

Simulations considering an adsorbent capacity loss over the years show that the capacity loss decreases the recovery of *p*-xylene in the unit. By considering an adsorbent capacity loss between 10 and 20% in the most recent case (Case C), it is observed that the fitting between the simulations and the industrial data improves.

UOP has recently launched ADS-47 as a drop-in replacement for the existing ADS-27 and ADS-37 adsorbents, resulting in low capital costs for capacity additions. UOP claims up to 50% capacity increase in existing units and 5–20% improved energy efficiency.[53] The revamping of Parex units is thus likely to occur in the near-to-medium future, and model-based tools, such as ours, will be of valuable help to the engineering team handling the project.

Acknowledgment

Marta S.P. Silva gratefully acknowledges the financial support from *Fundação para a Ciência e Tecnologia* (Ministry of Science and Technology of Portugal) for her Ph.D. scholarship SFRH/BDE/33836/2009.

Notation

A = rate of simulated circulation of the selective adsorbent pore volume, m^3/h
C = bulk liquid concentration, mol/m^3
C_p = fluid-phase concentration in the macroporous volume of the pellets, mol/m^3
CSS = cyclic steady state
D_{ax} = axial dispersion coefficient, m^2/s

D = diameter, m
DC = desorbent consumption, kg of *p*-diethylbenzene/kg of *p*-xylene obtained in the extract
EO = extract out
EOP = extract outlet position
$f_F^a = Q_F^a/Q_F$
$f_F^{project} = Q_F/Q_F^{project}$
f_H^{line} = fraction of the bed line washed by the primary flush stream
f_X^{line} = fraction of the bed line washed by the secondary flush (or recycle) stream
FIP = feed inlet position
H_i = primary flush in stream
H_o = primary flush out stream
k = overall mass-transfer coefficient, s^{-1}
K = Langmuir constant, m^3/mol
L = length, m
Q_I = flow rate of Zone I, m^3/h
Q_{II} = flow rate of Zone II, m^3/h
Q_{IIA} = flow rate of Zone IIA, m^3/h
Q_{IIB} = flow rate of Zone IIB, m^3/h
Q_{III} = flow rate of Zone III, m^3/h
Q_{IIIA} = flow rate of Zone IIIA, m^3/h
Q_{IV} = flow rate of Zone IV, m^3/h
L_{II} = $LII = L_{II} + W$
L_{III} = $LIII = L_{III} + W$
L_{IV} = $LIV = L_{IV} + W$
m = mass, kg
N_k = number of columns in each zone (k=I, II, IIB, IIA, III, IIIA or IV)
NC = number of components
Pe = Péclet number
P = pressure, kg/cm^2
P_z = port/stream position (z=E, X, H_i, F, R, D or H_o)
PA = pumparound
PR = productivity, kg of *p*-xylene obtained in the extract/h m^3 of adsorbent
PUX = purity, %
Q = flow rate, m^3/h
q_m = saturation capacity, mol/kg of adsorbent
q^* = adsorbed concentration in equilibrium with the intraparticle fluid, mol/kg adsorbent
R_p = pellet radius, m
REX = recovery, %
SMB = simulated moving bed
$step_{cycle}$ = step of the cycle ($1 < step_{cycle} < 24$)
t = time, s
t^* = switching time, s
t_c = cycle time, s
TMB = true moving bed
u = interstitial velocity, m/s
u_{solid} = solid interstitial velocity, m/s
V = volume, m^3
V_s = selective volume, m^3
V_w = nonselective volume, m^3
W = rate of simulated circulation of the nonvolume, m^3/h
z = axial coordinate

Greek symbols

ε_b = bulk porosity, V_b/V_c
ε_b' = extra column porosity, $(V_b+V_{extra})/V_c$
ε_p = particle macroporosity, V_p/V_{ads}
ρ = liquid density, kg/m^3
ρ_b = bulk density, kg/m^3
ρ_p = apparent density, kg/m^3
ξ = adsorption capacity loss, %/year

Subscripts and superscripts

0 = initial
a = aromatic fraction
ads = adsorbent
BH = bed head
c = Column
ch = adsorbent chamber
circ = circulation line
D = desorbent stream
dead = dead volume
E = extract stream
F = Feed stream
H = primary flush stream
in = inlet position of the column
line = bed line
out = outlet position of the column
R = raffinate stream
X = recycle or secondary flush stream
p-x = *p*-xylene
m-x = *m*-xylene
o-x = *o*-xylene
eb = ethylbenzene
p-deb = *p*-diethylbenzene
N/A = nonaromatics
tol = toluene

Literature Cited

1. Cannella WJ. *Xylenes and Ethylbenzene*. New York: Wiley, 2000.
2. Washburn EW. *International Critical Tables of Numerical Data, Physics, Chemistry and Technology*, 1st ed. London: Knovel, Reed Elsevier, 2003.
3. Meyers RA. *Handbook of Petroleum Refining Processes*, 3rd ed. New York: McGraw-Hill, 2003.
4. Minceva M, Gomes PS, Meshko V, Rodrigues AE. Simulated moving bed reactor for isomerization and separation of *p*-xylene. *Chem Eng J*. 2008;140:305–323.
5. Broughton DB, Gerhold CG. Continuous sorption process employing fixed bed of sorbent and moving inlets and outlets. Universal Oil Products. US 2985589 A, 1961.
6. Parex™—Aromatics, UOP LLC. Available at: www.uop.com, 2006. Accessed on January, 2013.
7. Priegnitz J, Johnson D, Cheng L, Comissaris S, Hurst J, Quick M, Kulprathipanja S. Binderless adsorbents with improved mass transfer properties and their use in the adsorptive separation of para-xylene. US 7820869 B2, UOP LLC, 2010.
8. Gembicki S, Johnson J. The role of adsorption in meeting future energy challenges. In: *9th International Conference on Fundamentals of Adsorption*, Sicily, Italy, 2007.
9. Minceva M, Rodrigues AE. Understanding and revamping of industrial scale SMB units for p-xylene separation. *AIChE J*. 2007;53:138–149.
10. Broughton DB, Neuzil RW, Pharis JM, Brearley CS. The Parex process for recovering paraxylene. *Chem Eng Prog*. 1970;66:70–75.
11. Migliorini C, Mazzotti M. Simulated moving bed with extra-column dead volume. *AIChE J*. 1999;45:1411–1421.
12. Grosfils V. Modelling and parametric estimation of simulated moving bed chromatographic processes (SMB). PhD Thesis. Université Libre de Bruxelles, Brussle, Belgium, 2009.
13. Katsuo S, Langel C, Schanen P, Mazzotti M. Extract-column dead volume in simulated moving bed separations: theory and experiments. *J Chromatogr A*. 2009;1216:1084–1093.
14. Minceva M, Rodrigues AE. UOP's Parex: Modeling, Simulation and Optimization. In: *ENPROMER—2nd Mercosur Congress on Chemical Engineering/4th Mercosur Congress on Process Systems Engineering*, Brasil, 2005.
15. Minceva M, Rodrigues AE. Influence of the transfer line dead volume on the performande of an industrial scale simulated moving bed for p-xylene separation. *Sep Sci Technol*. 2003;38:1463–1497.
16. Lim Y-I, Lee J, Bhatia SK, Lim Y-S, Han C. Improvement of para-xylene SMB process performance on an industrial scale. *Ind Eng Chem Res*. 2010;49:3316–3327.
17. Sutanto PS, Lim Y-I, Lee J. Bed-line flushing and optimization in simulated moving-bed recovery of para-xylene. *Sep Purif Technol*. 2012;96:168–181.
18. Carson DB, Purse FV, *Rotary Valve, Universal Oil Products Company*, US 3040777 A, 1962.
19. Chiang AST. Equilibrium theory for simulated moving bed adsorption processes. *AIChE J*. 1998;44:2431–2441.
20. Mazzotti M, Storti G, Morbidelli M. Robust design of binary countercurrent separation processes: 3. Nonstoichiometric systems. *AIChE J*. 1996;42:2784–2796.
21. Nicolaos A, Muhr L, Gotteland P, Nicoud R-M, Bailly M. Application of the equilibrium theory to ternary moving bed configurations (four+four, five+four, eight and nine zones) I. Linear case. *J Chromatogr A*. 2001;908:71–86.

22. Zhong G, Guiochon G. Analytical solution for the linear ideal model of simulated moving bed chromatography. *Chem Eng Sci*. 1996;51: 4307–4319.
23. Yun T, Zhong G, Guiochon G. Simulated moving bed under linear conditions: experimental vs. calculated results. *AIChE J*. 1997;43: 935–945.
24. Zhong G, Smith M, Guiochon G. Effect of the flow rates in linear, ideal, simulated moving-bed chromatography. *AIChE J*. 1997;43: 2960–2969.
25. Ruthven D. *Principles of Adsorption and Adsorption Processes*. New York: Wiley, 1984.
26. Ganetsos G, Barker PE. Preparative and production scale chromatography. In: *Chromatographic Science Series*. New York: Marcel Dekker, 1993.
27. Silva MSP, Mota JPB, Rodrigues AE. Fixed-bed adsorption of aromatic C8 isomers: breakthrough experiments, modeling and simulation. *Sep Purif Technol*. 2012;90:246–256.
28. Silva MSP, Moreira MA, Ferreira AFP, Santos JC, Silva VMTM, Sá Gomes P, Minceva M, Mota JPB, Rodrigues AE. Adsorbent evaluation based on experimental breakthrough curves: separation of p-xylene from C8 isomers. *Chem Eng Technol*. 2012;35:1777–1785.
29. Silva MSP, Mota JPB, Rodrigues AE. Adsorption equilibrium and kinetics of the Parex's feed and desorbent streams from batch experiments. *Chem Eng Technol*. 2014;37:1541–1551.
30. Glueckauf E. Theory of chromatography. Part 10. Formulae for diffusion into spheres and their application to chromatography. *Trans Faraday Soc*. 1955;51:1540–1551.
31. Azevedo DCS, Rodrigues AE. Design of a simulated moving bed in the presence of mass-transfer resistances. *AIChE J*. 1999;45:956–966.
32. Ching CB, Ruthven DM. An experimental study of a simulated counter-current adsorption system—I. Isothermal steady state operation. *Chem Eng Sci*. 1985;40:877–885.
33. Gomes PS, Minceva M, Rodrigues AE. Operation of an industrial SMB unit for p-xylene separation accounting for adsorbent ageing problems. *Sep Sci Technol*. 2008;43:1974–2002.
34. Hassan MM, Rahman AKMS, Loughlin KF. Numerical simulation of unsteady continuous countercurrent adsorption system with nonlinear adsorption isotherm. *Sep Technol*. 1994;4:15–26.
35. Hidajat K, Ching CH. Simulation of the performance of a continuous counter-current adsorption system by the method of orthogonal collocation with non-linear and interacting adsorption isotherms. *Trans IChemE*. 1990;68:104–108.
36. Minceva M, Rodrigues AE. Modeling and simulation of a simulated moving bed for the separation of p-xylene. *Ind Eng Chem Res*. 2002;41:3454–3461.
37. Pais LS, Loureiro JM, Rodrigues AE. Modeling, simulation and operation of a simulated moving bed for continuous chromatographic separation of 1,1′-bi-2-naphthol enantiomers. *J Chromatogr A*. 1997; 769:25–35.
38. Zabka M, Gomes PS, Rodrigues AE. Performance of simulated moving bed with conventional and monolith columns. *Sep Purif Technol*. 2008;63:324–333.
39. Pais LS, Loureiro JM, Rodrigues AE. Modeling strategies for enantiomers separation by SMB chromatography. *AIChE J*. 1998; 44:561.
40. Gomes PS, Zabkova M, Zabka M, Minceva M, Rodrigues AE. Separation of chiral mixtures in real SMB units: the flexSMB-LSRE. *AIChE J*. 2010;56:125–142.
41. Hassan MM, Rahman AKMS, Loughlin KF. Modelling of simulated moving bed adsorption systems: a more precise approach. *Sep Technol*. 1995;5:77–89.
42. Lim BG, Ching CB. Modelling studies on the transient and steady state behaviour of a simulated counter-current chromatographic system. *Sep Technol*. 1996;6:29–41.
43. Lim Y, Lee J, Bhatia SK, Han C. Improvement of para-xylene SMB process performance on an industrial scale. *Ind Chem Res*. 2010;49: 3316–3327.
44. Lu ZP, Ching CB. Dynamics of simulated moving-bed adsorption separation processes. *Sep Sci Technol*. 1997;32:1993–2010.
45. Migliorini C, Gentilini A, Mazzotti M, Morbidelli M. Design of simulated moving bed units under nonideal conditions. *Ind Eng Chem Res*. 1999;38:2400–2410.
46. Mota JPB, Araújo JMM. Single-column simulated-moving-bed process with recycle lag. *AICHE J*. 2005;51:1641–1653.
47. Rodrigues AE, Dias MM. Linear driving force approximation in cyclic adsorption processes: simple results from system dynamics based on frequency response analysis. *Chem Eng Process*. 1998;37: 489–502.
48. Azevedo DCS, Rodrigues AE. Bilinear driving force approximation in modeling of a simulated moving bed using bidisperse adsorbents. *Ind Eng Chem Res*. 1999;38:3519–3529.
49. Neuzil R. Process for separating para-xylene. US 3997620, UOP, 1976.
50. Storti G, Mazzotti M, Morbidelli M, Carra S. Robust design of binary countercurrent adsorption separation processes. *AIChE J*. 1993;39:471.
51. Mazzotti M, Storti G, Morbidelli M. Optimal operation of simulated moving bed units for nonlinear chromatographic separations. *J Chromatogr A*. 1997;769:3.
52. Mazzotti M. Equilibrium theory based design of simulated moving bed processes for a generalized Langmuir isotherm. *J Chromatogr A*. 2006;1126:311.
53. Brookes T. New Technology Developments in the Petrochemical Industry. In: *Echem/Petroleum Economist Egypt Petrochemical Conference*, Cairo, Egypt, 2012.

Manuscript received Sep. 7, 2014, and revision received Dec. 9, 2014.